Coordination Chemistry Reviews, 109 (1991) 1–59
Elsevier Science Publishers B.V., Amsterdam

COMPLEX FORMATION OF THE LANTHANIDES AND ACTINIDES IN LOWER OXIDATION STATES

N.B. MIKHEEV* and A.N. KAMENSKAYA

Institute of Physical Chemistry, Academy of Sciences of U.S.S.R., 31 Leninsky Prospekt, 117915 Moscow (U.S.S.R.)

(Received 13 March 1990)

CONTENTS

A. List of abbreviations 1
B. Preface 2
C. Lower oxidation states of the lanthanides and actinides 4
D. The cocrystallization method and its application for the study of complex compounds of the lanthanides and actinides 11
E. Hydration and solvation of the divalent lanthanides and actinides 20
(i) Hydration of Ln^{2+} and An^{2+} ions 20
(ii) Solvation–hydration interaction between Eu^{2+}, Yb^{2+}, Es^{2+} and aqueous-ethanolic solutions 22
(iii) Complex formation of the lanthanides and actinides in their lower oxidation states with halide ions 26
F. Coordination compounds of the lanthanides and actinides in their lower oxidation states with organic ligands 32
(i) Complex formation of Eu^{2+}, Yb^{2+} and Es^{2+} with the tetraphenylborate ion 33
(ii) Complex formation of lanthanides and actinides in their lower oxidation states with neutral macrocyclic polyethers 37
(a) Complex formation of Ln^{2+} and An^{2+} with macrocyclic polyethers in solution . . 37
(b) Complex formation of uranium(III) with crown ethers 42
G. Solid coordination compounds of the lanthanides and actinides in their lower oxidation states 43
(i) Ln^{2+} and U^{3+} compounds with crown ethers 46
H. Coordination chemistry of Ln^{2+} and An^{2+} with an $f^{n-1}d^1$-configuration 48
(i) Simple clusters of divalent plutonium and curium 49
(ii) Condensed lanthanide and actinide clusters 51
(a) Mixed condensed lanthanide and actinide clusters of the M_2Cl_3 type 52
I. Conclusion 57
References 57

A. LIST OF ABBREVIATIONS

Ln	lanthanides
An	actinides

* To whom correspondence should be addressed.

0010–8545/91/$20.65

X	halides
EDTA	ethylenediaminetetraacetic acid
HMPA	hexamethylphosphoric triamide
THF	tetrahydrofuran
PC	propylene carbonate
TPB	tetraphenylborate
18C6	18-crown-6
DB18C6	dibenzo-18-crown-6
DBB18C6	dibutylbenzo-18-crown-6
DT18C6	dithia-18-crown-6
DA18C6	diaza-18-crown-6
DCH18C6	dicyclohexyl-18-crown-6
12C4	12-crown-4
15C5	15-crown-5
BB15C5	4-*tert*-butylbenzo-15-crown-5
DB30C10	dibenzo-30-crown-10
Cp	cyclopentane
Fc	ferrocene
Et_2O	diethyl ether

B. PREFACE

Most of the lanthanides and actinides in the form of free neutral atoms have an $f_n s^2$ electron configuration. If *f*-electrons are regarded as inner ones, which are not involved in establishing chemical bonds, such an electron configuration is analogous to that of alkaline earth metals. At the same time, the main oxidation state of the majority of *f*-elements is 3+. The reason for the instability of the divalent state is that the difference in the hydration energies of tri- and divalent lanthanide and actinide ions exceeds the ionization energies of doubly charged ions. This difference decreases when transmitting from water to solvents with a lower dielectric constant, and therefore in non-aqueous solvents the stability of divalent lanthanides increases. Thus, the problem of the stability of divalent lanthanides and actinides is closely related to the coordination chemistry of these elements.

Since the divalent lanthanides and actinides are mainly formed through reduction of their trivalent forms, it seems of interest to consider briefly the complex formation of Ln^{3+} and An^{3+}. Trivalent actinides, and especially lanthanides, are known to be weak complex formers. The main contribution to the complex formation of the elements is due to electrostatic interaction. To a certain extent, the complex formation process is accounted for by the overlapping of *f*-orbitals and ligand orbitals, e.g. when complexes of the chelate type are formed [1].

Antibonding effects, which do not vary monotonically with change in the number of *f*-electrons, are believed to be of primary importance during the formation of covalent bonds in rare earth complexes. Apart from the antibonding effects, the ligand geometry and inhomogeneity of the coordination sphere, which is due to the competing role of the ligand and solvent, are also significant with respect to the formation and stability of the complexes.

Since, in the case of the actinides, spin-orbital coupling is more important than in the case of the lanthanides, the stability of actinide complexes is higher than that of lanthanide complexes of similar composition.

The energy of *f*-orbitals is determined by such factors as electrostatic interaction, which makes the greatest contribution, spin-orbital coupling and the crystal field effect. For solutions of trivalent lanthanides and actinides, these energy parameters are easy to determine from the absorption spectra of the Laporte-forbidden *f–f* transitions [2,3].

When the lanthanides and actinides transit from the trivalent to the divalent state, an increase in the energy of the electrons in their *f*-orbitals occurs. However, the influence of this effect on complex formation of Ln^{2+} and An^{2+} is not yet well understood.

Absorption spectra for the divalent lanthanides have not yet been interpreted since, along with low-intensity *f–f* transitions, they contain very intense broad *f–d* bands. Nevertheless, certain information on the interaction between the Ln^{2+} ion and the environment with respect to varying the solvent may be obtained from the *f–d* transitions.

To interpret the spectra of *f–d* transitions for Ln^{2+} in a crystalline matrix, Johnson and Sandoe suggested a scheme of $J_1\gamma$-interaction, where J_1 is the quantum number of the f^{n-1} configuration in the Russell-Saunders approximation, and $J_1\gamma$ is the state of the *d*-electron in the crystal field [4]. This interaction scheme was used for interpreting the spectra of *f–d* transitions for Ln^{2+} in solution [5,6]. Such energy parameters as the crystal field splitting parameter (Δ) and the energy of the first unsplit level of the Ln^{2+} *fd*-configuration (E_{fd}) were determined in various systems using this scheme.

For a long time, the complex formation abilities of Ln^{2+} and An^{2+} involved only those of No^{2+} and Eu^{2+} which are stable in aqueous solution. Silva et al. [7] and McDowell et al. [8] showed that No^{2+} was in many respects similar to Ca^{2+} and Sr^{2+}, especially with regard to extraction, ion exchange and complex formation with oxyacids. These abilities of No^{2+} are accounted for by the filled 5*f*-orbital, and in the case of Eu^{2+}, by a half-filled 4*f*-shell (f^7). Owing to the relative stability of Eu^{2+} in aqueous solutions, some of its quantitative complex formation characteristics were obtained [9,10].

The behaviour of Eu^{2+} regarding complexons [11] has been studied systematically using polarography and pH-potentiometry methods. The forma-

tion of protonated and normal Eu^{2+} complexes with a number of complexons has been established and the stability constants determined. The latter appeared to be much lower than those of the respective Eu^{3+} complexes. The strongest Eu^{2+} complexes are those with ethylenediaminetetraacetic acid (EDTA), diethylenepentaacetic acid (DEPA), hydroxyethylendiaminetetraacetic (HEDTA) and ethylenediaminediisopropylphosphonic (DETAIPP) acids ($\log \beta \approx 10$). In most cases, the values of these constants lie between those for the respective complexes of Ca^{2+} and Sr^{2+}, which points to a similarity between Eu^{2+} and alkaline earth elements.

Recently, information became available to undertake a broader comparison of the properties of Ln^{2+} and An^{2+} with alkaline earth ions; this reveals both the similarities and differences between them as well as other elements of the Mendeleev periodic system. These data are of indubitable interest for the development of the periodic law.

C. LOWER OXIDATION STATES OF THE LANTHANIDES AND ACTINIDES

For a long time the three lanthanides Eu, Yb and Sm were known to exist in their divalent states. The dihalides of these elements are obtained by reducing their trihalides with hydrogen at higher temperatures. Tm, Dy, Nd, Pr and Ho are much more difficult to reduce. Dihalides of these metals are obtained through reactions between trihalides (chlorides, bromides and iodides) and the respective metals in melts. Moreover, the formation of Pr and Ho dihalides will not go to completion and these dihalides are not obtained in the pure form. A detailed study of the systems $Ln-LnX_3$ was carried out by Corbett and coworkers and their results were generalized by Braun [12]. They succeeded in discovering a number of mixed phases containing LnX_2 in different proportions with LnX_3. In recent years, the properties of halides, oxyhalides and oxides of lanthanides in lower oxidation states have been studied intensively by Meyer and coworkers and Bärninghausen and coworkers [13–16].

Am and Cf dihalides were obtained in the solid state [17–19]. Data are also available for Es dihalides and their absorption spectra [19]. All the transeinsteinium elements are obtainable in submicrogram quantities and, therefore, they are not known to exist in the solid state in the form of independent dihalide phases. At present, all the lanthanides from La to Lu and the actinides from U to No have been obtained in solution and melts in the oxidation state 2+ [20,21]. Table 1 presents the values of standard oxidation potentials $E^0_{M^{3+}/M^{2+}}$ [20–23]. The table also contains oxidation potentials calculated by Vander Sluis and Nugent [22]. Their theoretical calculations are based on the correlation between the oxidation potential of an element and its f–d excitation energy. There is satisfactory agreement

TABLE 1

Oxidation potentials $E^0_{M^{3+}/M^{2+}}$ for the lanthanides and actinides (NHE)

Ln	$E^0_{Ln^{3+}/Ln^{2+}}$			An	$E^0_{An^{3+}/An^{2+}}$	
	Ref. 20	Ref. 22	Ref. 23		Ref. 20	Ref. 22
La	-2.94 ± 0.08	-3.1 ± 0.2		Ac	Unknown	-4.9 ± 0.2
Ce	-2.92 ± 0.08	-3.2 ± 0.2		Th	Unknown	-4.9 ± 0.2
Pr	-2.84 ± 0.06	-2.7 ± 0.2		Pa	Unknown	-4.7 ± 0.2
Nd	-2.62 ± 0.05	-2.6 ± 0.2	-2.6	U	-2.60 ± 0.06	-4.7 ± 0.2
Pm	-2.44 ± 0.06	-2.6 ± 0.2		Np	-2.83 ± 0.07	-4.7 ± 0.2
Sm	-1.50 ± 0.01	-1.6 ± 0.2	-1.55	Pu	-2.79 ± 0.07	-3.5 ± 0.2
Eu	-0.34 ± 0.01	-0.3 ± 0.2	-0.35	Am	-2.28 ± 0.06	-2.3 ± 0.2
Gd	-2.85 ± 0.07	-3.9 ± 0.2		Cm	-2.78 ± 0.07	-4.4 ± 0.2
Tb	-2.83 ± 0.07	-3.7 ± 0.2		Bk	-2.25 ± 0.06	-2.8 ± 0.2
Dy	-2.56 ± 0.05	-2.6 ± 0.2	-2.5	Cf	-1.63 ± 0.02	-1.6 ± 0.2
Ho	-2.79 ± 0.06	-2.9 ± 0.2		Es	-1.45 ± 0.02	-1.3 ± 0.2
Er	-2.87 ± 0.08	-3.1 ± 0.2		Fm	-1.18 ± 0.02	-1.1 ± 0.2
Tm	-2.22 ± 0.05	-2.3 ± 0.2	-2.3	Md	-1.15 ± 0.01	-0.0 ± 0.2
Yb	-1.18 ± 0.01	-1.1 ± 0.2	-1.05	No	$+1.45$	$+1.3\pm0.2$
Lu	-2.72 ± 0.07			Lw	Unknown	

between the calculated and experimental values for oxidation potentials of the elements with high *f–d* excitation energy values. On the other hand a noticeable divergence is observed in the case of the elements with low *f–d* transition energies. This divergence is especially noticeable in the case of Cm, Pu, Tb and some other elements. Tables 2 and 3 show values of the *f–d* excitation energy for free neutral atoms and free doubly charged ions, together with their electronic configurations and orbital terms. Based on the terms of the total orbital moment, each of the families of *f*-elements may be divided into two sub-families, with the respective elements of the first and second halves of the lanthanides and second half of the actinides having the same terms (which differ only in multiplicity). At the same time, elements of the first half of the actinides are beyond our consideration because they have other terms and because their chemical properties are close to those of *d*-elements.

When considering the dependence of the oxidation potential on the *f–d* excitation energy (Figs. 1–3) for the elements of the first and second halves of the lanthanides and the second half of the actinides, one should note a linear relationship between these two parameters for elements with high *f–d* excitation values and to the absence of the dependence $E^0 = f(E_{fd})$ for elements with low excitation energies.

The standard oxidation potential $E^0_{M^{3+}/M^{2+}}$ depends on the ionization

TABLE 2

Electronic configurations and terms corresponding to the basic states and energy of $f^n d^1 s^2$-configuration relative to the energy of $f^{n+1}s^2$-configuration for neutral atoms of the lanthanides and actinides [21,22]

Ln	Electronic configuration	Term	E_{fd} (10^3 cm^{-1})	An	Electronic configuration	Term	E_{fd} (10^3 cm^{-1})
La	$[Xe]ds^2$	$^2D_{3/2}$	−15.20	Ac	$[Rn]ds^2$	$^2D_{3/2}$	−30
Ce	fds^2	$^1G_4$	−4.76	Th	d^2s^2	$^3F_2$	−49
Pr	f^2s^2	$^4I_{9/2}$	4.43	Pa	f^2ds^2	$^4K_{11/2}$	−11.44
Nd	f^4s^2	$^5I_4$	6.76	U	f^3ds^2	$^5L_6$	−7.02
Pm	f^5s^2	$^6H_{5/2}$	8.00	Np	f^4ds^2	$^6L_{11/2}$	−1
Sm	f^6s^2	$^7F_0$	13.80	Pu	f^6s^2	$^7F_0$	6.31
Eu	f^7s^2	$^8S_{7/2}$	25.1	Am	f^7s^2	$^8S_{7/2}$	17
Gd	f^7ds^2	$^9D_2$	−10.95	Cm	f^7ds^2	$^9D_2$	−1.21
Tb	f^9s^2	$^6H_{15/2}$	0.29	Bk	f^9s^2	$^6H_{15/2}$	7.4
Dy	$f^{10}s^2$	$^5I_8$	7.57	Cf	$f^{10}s^2$	$^5I_8$	17
Ho	$f^{11}s^2$	$^4I_{15/2}$	8.38	Es	$f^{11}s^2$	$^4I_{15/2}$	19
Er	$f^{12}s^2$	$^3H_6$	7.18	Fm	$f^{12}s^2$	$^3H_6$	20
Tm	$f^{13}s^2$	$^2F_{7/2}$	13.12	Md	$f^{13}s^2$	$^2F_{7/2}$	30
Yb	f^{14}	$^1S_0$	23.19	No	$f^{14}s^2$	$^1S_0$	37

TABLE 3

Electronic configurations and terms corresponding to the ground states and energy of the $f^n d^1$-configuration relative to the energy of the f^{n+1}-configuration for doubly-charged ions of the lanthanides and actinides [21,22]

Ln	Electronic configuration	Term	E_{fd} (10^3 cm^{-1})	An	Electronic configuration	Term	E_{fd} (10^3 cm^{-1})
La	$[Xe]d^1$	$^2D_{3/2}$	−8.58	Ac	$[Rn]s^1$	$^2S_{1/2}$	−27.7
Ce	f^2	$^3H_4$	3.42	Th	d^2	$^3F_2$	−15.1
Pr	f^3	$^4I_{9/2}$	12.58	Pa	f^2d	$^4I_{11/2}$	−4.6
Nd	f^4	$^5I_4$	13.88	U	f^3d	$^5L_6$	0.0
Pm	f^5	$^6H_{5/2}$	14.85	Np	f^5	$^6H_{5/2}$	4.1
Sm	f^6	$^7F_0$	23.48	Pu	f^6	$^7F_0$	13.7
Eu	f^7	$^8S_{7/2}$	34.62	Am	f^7	$^8S_{7/2}$	23.9
Gd	f^7d	$^9D_2$	−2.19	Cm	f^8	$^7F_6$	7.1
Tb	f^9	$^6H_{15/2}$	9.40	Bk	f^9	$^6H_{15/2}$	18.9
Dy	f^{10}	$^5I_8$	17.52	Cf	f^{10}	$^5I_8$	27.8
Ho	f^{11}	$^4I_{15/2}$	16.87	Es	f^{11}	$^4I_{15/2}$	30.2
Er	f^{12}	$^3H_6$	15.80	Fm	f^{12}	$^3H_6$	32.2
Tm	f^{13}	$^2F_{7/2}$	23.12	Md	f^{13}	$^2F_{7/2}$	40.1
Yb	f^{14}	$^1S_0$	33.84	No	f^{14}	$^1S_0$	50.4

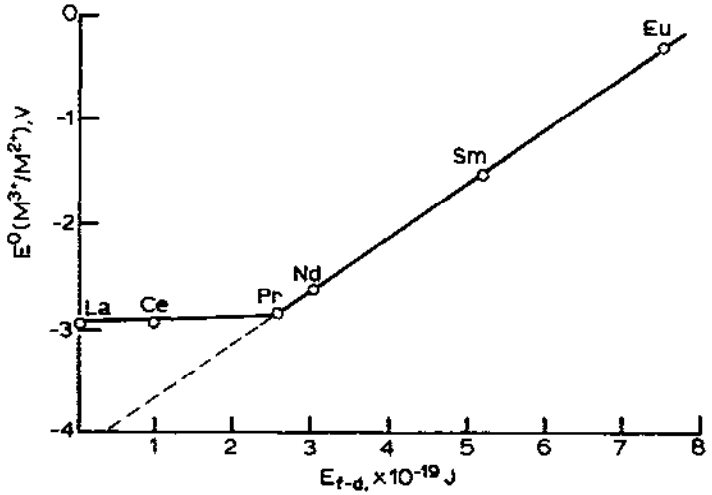

Fig. 1. Dependence of the standard M^{3+}/M^{2+} oxidation potential on the *f–d* excitation energy for the first half of the lanthanides [21].

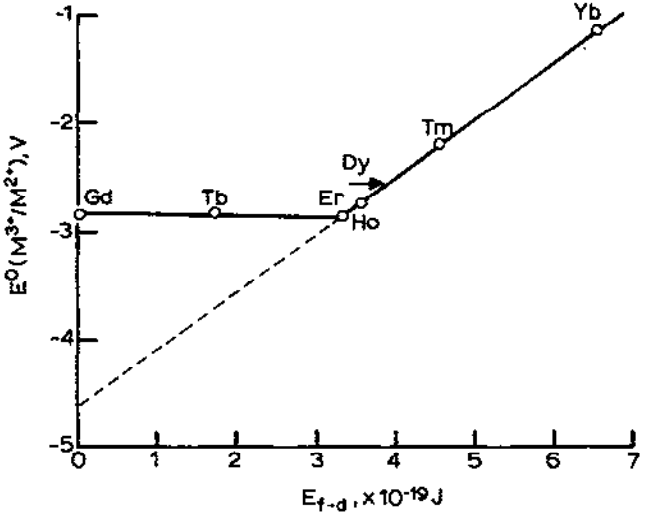

Fig. 2. Dependence of the standard M^{3+}/M^{2+} oxidation potential on the *f–d* excitation energy for the second half of the lanthanides [21].

energy and the hydration energy of doubly charged ions of an element according to

$$E^0_{M^{3+}/M^{2+}} + 4.43 = \Delta G^0_{ion} + \Delta G^0_{hydr}(M^{3+}) - \Delta G^0_{hydr}(M^{2+}) \quad (1)$$

where 4.43 V is the standard thermodynamic potential of the hydrogen electrode, ΔG^0_{ion} is the energy of the third ionization stage, and

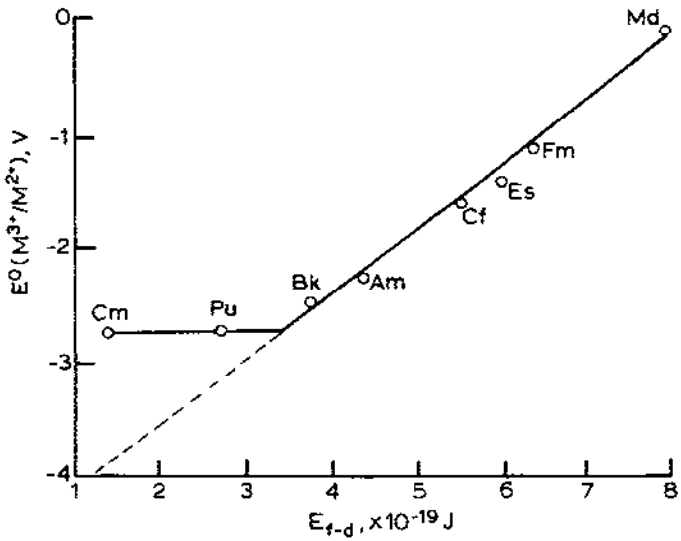

Fig. 3. Dependence of the standard M^{3+}/M^{2+} oxidation potential on the f–d excitation energy for the actinides [21].

$\Delta G^0_{hydr}(M^{2+})$ and $\Delta G^0_{hydr}(M^{3+})$ are the hydration energies of di- and trivalent ions.

Presenting the ionization energy from the main level as a sum of f–d excitation energies (E_{fd}) and the ionization energy from the high d-level (ΔG^0_{id}), eqn. (1) can be written

$$E^0_{M^{3+}/M^{2+}} = E_{fd} + [\Delta G^0_{Id} + \Delta G^0_{hydr}(M^{3+}) - \Delta G^0_{hydr}(M^{2+})] - 4.43 \quad (2)$$

Thus, the linear dependence $E^0_{M^{3+}/M^{2+}} = f(E_{fd})$ will be realized if the sum in the square brackets is constant or changes linearly with the chaning f–d excitation energy.

Hence, agreement between the experimental data (Figs. 1–3) and eqn. (2) explains the linear dependence of $E^0_{M^{3+}/M^{2+}}$ on E_{fd}. Obviously, in the case where there is no such dependence, the E_{fd} term is equal to 0. This occurs if the electron is localized not in the f- but in the d-orbital.

If, for example, one compares Gd and Tb, it follows from Table 1 that their oxidation potentials are practically identical though as free ions they have different electronic configurations (Table 2). In the ground state, Gd^{2+} has an $[f^7d^1]$ configuration, while Tb^{2+} has an $[f^9d^0]$ configuration, its f–d excitation energy being ≈ 1.4 eV [22]. This apparent discrepancy is accounted for by the fact that in a coordinated state, both these elements have the same electronic configuration $[f^nd^1]^{2+}$, which is possible when the stabilization energy exceeds the f–d excitation energy. As was reported by Johnson and Sandoe [4], the splitting energy of the d-level in the case of

La^{2+} and Gd^{2+} in the CaF_2 matrix is 3 eV. Consequently, the stabilization energy is close to 1.5 eV and it exceeds the f–d excitation energy of Tb^{2+}. When extrapolating $E^0_{M^{3+}/M^{2+}} = f(E_{fd})$ to the zero value of E_{fd} (Figs. 1–3), one may obtain the stabilization potential and, since we speak about a one-electron transition, also the stabilization energy. For the first and second halves of the lanthanides and the second half of the actinides, it is equal to 1.78, 1.79, and 1.91 eV, respectively [21]. For several reasons, these values may be considered approximate; however, they adequately explain the results presented in Figs. 1–3.

Thus, all the Ln^{2+} and An^{2+} ions in the coordinated state are subdivided into two groups: the elements of one group have an $f^n d^0$ electronic configuration, and those of the other are $f^{n-1}d^1$. The elements of the first group are formal analogues of alkaline earth ions; the elements of the second group are analogues of divalent Y or Sc. Ln^{2+} and An^{2+} having an $f^n d^0$ electronic configuration have been studied most thoroughly.

When, in the 1940s, Seaborg [24,25] formulated his actinide conception, he put forward an idea about the far-reaching similarity between the elements of the second halves of the lanthanide and actinide families. Having assumed the existence of the pair analogy between the respective elements of the second halves of the two families, Seaborg predicted the existence of tetravalent Bk (an analogue of Tb) and divalent Md and No (analogues of Tm and Yb). However, greater similarity is observed in the stability of tetravalent Ce and Bk and divalent Sm and Md, and also Eu and No [26]. Knowing the standard oxidation potentials $E^0_{M^{3+}/M^{2+}}$ (Table 1), one can establish the dependence of their change on the increase in the atomic number of an element (Fig. 4). As a matter of fact, the curves referring to the elements of the first half of the lanthanides and the second half of the actinides are parallel, in contrast to the elements of the second half of the lanthanides. For the second half of the lanthanides, increasing atomic number leads to a non-monotonic change in the oxidation potential. This shows in the minimum stability of Er. Such similarity between the elements of the first half of the lathanides and the second half of the actinides shows the change of $E^0_{M^{4+}/M^{3+}} = f(Z)$ (Fig. 5).

Based on the data obtained, it can be concluded that, in the elements of the first half of the lanthanides and the second half of the actinides, there occurs a simbiotic change in the energy of the f-electrons with an increase in the atomic number, whether the f-orbital gains or loses an electron [26]. The similarity discovered between the elements of the first half of the lanthanides and the second half of the actinides only refers to the elements which, in their coordinated state, have an $[f^n d^0]^{2+}$ electronic configuration. As far as the elements with an $[f^{n-1}d^1]^{2+}$ electronic configuration are concerned, the chemical properties characteristic of compounds with such a configuration

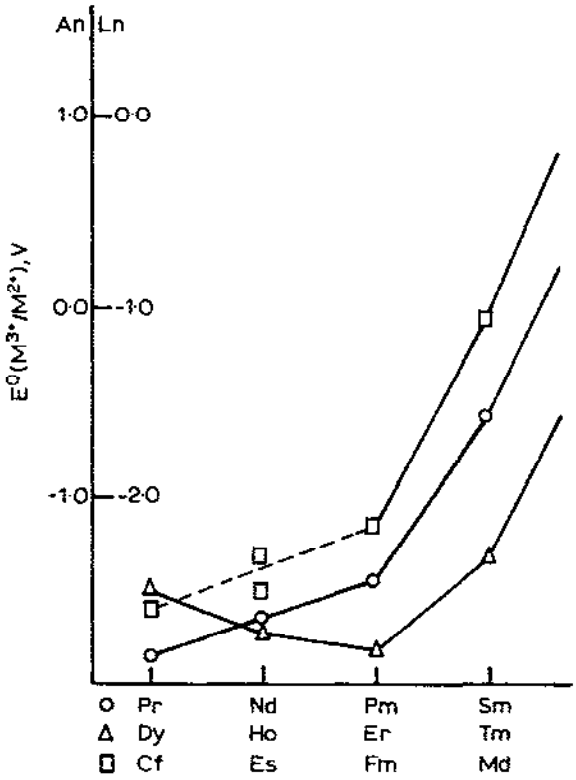

Fig. 4. Dependence of the change in $E^0_{M^{3+}/M^{2+}}$ on the atomic number of the elements for the lanthanides and actinides [20].

have been insufficiently studied. The scarce information available will be considered further.

The similarity between the respective elements of the first half of lanthanides and the second half of actinides is of special interest for studying the far actinides. All the elements belonging to the second half of the actinides have been obtained artificially, with many of them being highly radioactive, thereby limiting their investigation. Another difficulty is in the short lifetime of the elements in question. This mainly refers to No, Md and Fm. Studying the chemistry of these elements, when the researcher has to deal with either millions or several atoms, is impossible using traditional methods. The duration of the experiments is not the least factor in such investigations because the half-lives of the above elements vary from hours to minutes. Therefore, studying the coordination chemistry of far actinides is limited to solutions, and the methods employed are based on migration processes, e.g. electromigration or phase distribution.

The methods of liquid extraction and ion exchange, which are widely used

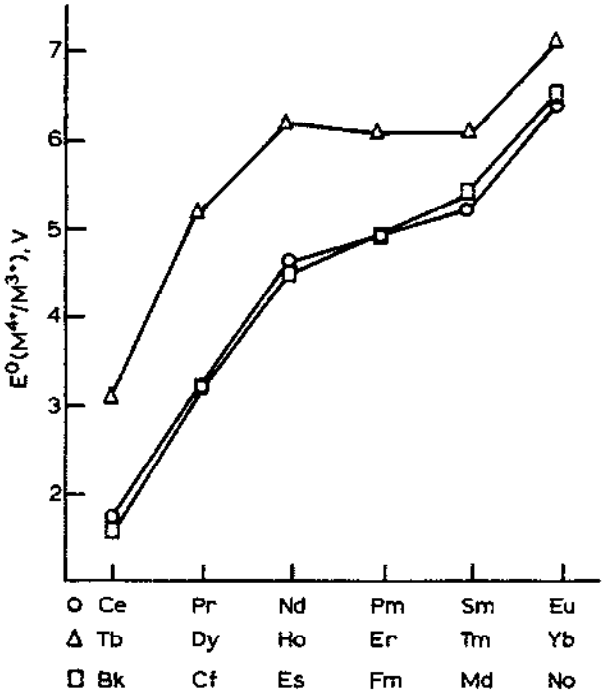

Fig. 5. Dependence of the change in $E^0_{M^{4+}/M^{3+}}$ on the atomic number of the elements for the lanthanides and actinides [20].

for the study of stability constants and composition of complex compounds in aqueous solutions, prove to be of no use for studies on the coordination chemistry of elements dissolved in organic solvents. However, it is organic solvents with which we have to deal when studying lower oxidation states of the lanthanides and the actinides, as these elements exhibit the greatest stability in organic solutions with low dielectric constant. Therefore cocrystallization is the most suitable method for studying their chemistry, including the coordination chemistry.

D. THE COCRYSTALLIZATION METHOD AND ITS APPLICATION FOR THE STUDY OF COMPLEX COMPOUNDS OF THE LANTHANIDES AND ACTINIDES

As mentioned above, there are three main factors hampering studies of the complex compounds of the far actinides in their lower oxidation states. These are the availability of the actinides only in ultramicroquantities, their short lifetimes and, finally, the necessity to use non-aqueous solution of these elements. But when the cocrystallization method is employed, all three conditions can be fulfilled.

Earlier, the cocrystallization method was used for separation purposes, and the use of complex formers was considered as a means of increasing the efficiency of separation. However, at present the cocrystallization method is being developed as a method of physico-chemical investigation of ultramicro-quantities of these elements.

The distribution of microcomponents between the solid and liquid phases in equilibrium is described by the Henderson–Kraček equation [27]

$$\frac{x}{y} = D\frac{a-x}{b-y} \tag{3}$$

where x and y are the quantities of micro- and macrocomponents in the solid phase, a and b are their content in the whole system, and D is the cocrystallization coefficient, independent of the relative quantities of the solid and liquid phases.

As was reported by Ratner [28], the cocrystallization coefficient depends on the properties of the components in solution and in the solid phase.

$$D = \frac{SP_M}{SP_m}\left(\frac{\gamma_{\pm(m)}}{\gamma_{\pm(M)}}\right)^{\nu} \exp\left(-\frac{\Delta\mu}{RT}\right) \tag{4}$$

where SP are the products of the solubilities of macrocomponent (M) and microcomponent (m), $\gamma_{\pm}$ are their activity coefficients in solution, ν is the number of ions resulting from the dissociation of salt, and $\exp(-\Delta\mu/RT)$ is the work required for the formation of the solid solution.

If the solid phase of the pure microcomponent is taken for the standard phase, the work required for the formation of the solid solution may be considered a measure of the deviation of the behaviour of the microcomponent from the ideal state

$$\exp\left(-\frac{\Delta\mu}{RT}\right) = \frac{1}{f} \tag{5}$$

where f is the activity coefficient of the microcomponent in the solid phase.

For simple salts, the f value, depending mainly on the difference in the interatomic distances of macro- and micro-components, may differ greatly from 1. Thus, for example, in the solid solution K(Cs)Cl, the activity coefficient of CsCl is equal to 21 [29,30]. On the other hand in the case of complex compounds, the interatomic distance increases considerably, and the value approaches 1. Due to this phenomenon, it becomes possible to determine the activity product for macro- and microcomponents.

This problem was successfully solved when the solubility product of the complex compound NaAmEDTA was determined on the basis of its cocrystallization with NaAmEDTA from a 50% solution of acetonitrile [31]. The

solubility product of NaAmEDTA, obtained through measurements of solubility, coincided with the solubility product value obtained in the experiments on cocrystallization with NaEuEDTA $(4.9 \pm 0.5) \times 10^{-6}$ and $(5.9 \pm 0.9) \times 10^{-6}$, respectively. A similar problem was resolved for lanthanide and actinide diiodide complexes with 18C6 which are poorly soluble in tetrahydrofuran [32]. The validity of this method was confirmed when the solubility of analogous salts of alkaline earth elements was determined. In all cases, the strontium diiodide salt with 18C6 was used as a matrix. However, the solubilities of calcium and barium salts were also determined directly by saturating the solution. As is seen in Table 4, both methods yielded very similar results.

The cocrystallization method was used not only to determine the solubility products of salts, but also to determine the ionic radius of the microelement.

Mikheev and coworkers [33] used the thermodynamic ground cocrystallization, developed by Urusov [34], for determining the solubility product of MdCl and the ionic radius of monovalent mendelevium. The Urusov equation establishes a relationship between the cocrystallization coefficient and the solubility product ratio and interatomic distances of components

$$\ln D = \ln \frac{SP_1}{SP_2} \frac{(t_m - T)a}{R_G T t_m} \left(\frac{R_1 - R_2}{R_1} \right)^2 \tag{6}$$

where SP is the solubility product of the components, R is the atomic distance, R_G is the gas constant, T is the absolute temperature, t_m is the correlation factor, and a is a constant.

TABLE 4

Solubility products (SP) $MI_2 \cdot 18C6$ in THF at 25 °C (10^{-12}) [32]

M^{2+}	SP calculated on the basis of D[a]	SP obtained from the solubility of complexes
Ca^{2+}	78 ±8	64 ±6
Sr^{2+}		6.5 ±0.6
Ba^{2+}	0.42 ± 0.04	0.44 ± 0.04
Sm^{2+}	5.9 ±0.5	
Eu^{2+}	6.3 ±0.3	
Yb^{2+}	7.9 ±1.0	
Am^{2+}	6.6 ±0.4	
Cf^{2+}	7.1 ±0.5	
Es^{2+}	7.1 ±0.5	
Fm^{2+}	6.8 ±0.7	

[a] SP = solubility product ($mol^3\ l^{-3}$); D = cocrystallization coefficient (dimensionless).

If the data for two different matrices are available, then one can determine the R value for Md^+ and SP for MdCl by solving two equations with two unknown members for the microcomponent. The solubility product of MdCl is close to that of KCl, and the ionic radius of Md^+ equals 0.117 nm, which is between the ionic radius values for K^+ and Na^+ (coordination number 6). These results show that Md^+ is chemically close to the alkaline metal ions.

Studies on the complex formation processes in solution with the use of the cocrystallization method suppose that the composition of the solid phase does not change when a complex former is introduced into solution. This condition is directly attributable to the fact that the macrocomponent either does not take part in complex formation with the ligands introduced or it is partially bound in the complex [35]. In the case where the macro- and microelements form only one complex, the equation

$$[A_M(tot)] = [A_M] + [A_MB] \tag{7}$$

is valid where $[A_M(tot)]$ is the total concentration of the macroelement in solution, and $[A_M]$ and $[A_MB]$ correspond to the concentration of the macroelement in simple ionic and complex states. Similarly, the concentrations of the microelement will be described by the equation

$$[A_m(tot)] = [A_m] + \{\beta_2[A_m][B]\} \tag{8}$$

where the first member is the concentration of the microelement in the ionic state, and the second its concentration in the complex state, β_2 is the stability constant for the complex state of the microcomponent, and [B] is the ligand concentration.

The ligand concentration [B] can be found if the ratio $[A_MB]/[A_M]$ is known:

$$[B] = \frac{[A_MB]}{\beta_1[A_M]} \tag{9}$$

where β_1 is the stability constant of the complex compound of the macroelement.

Equation (8) may be transformed in the following way:

$$[A_m(tot)] = [A_m]\left\{1 + \frac{\beta_2}{\beta_1}\frac{[A_MB]}{[A_M]}\right\} \tag{10}$$

Using in eqn. (3) the $[A_m]$ and $[A_M]$ values from eqns. (10) and (7) ($[A_m] = (a-x)/V$, $[A_M] = (b-y)/V$, and V = the liquid volume) we have:

$$D = \frac{x\{[A_M(tot)] - [A_MB]\}}{y[A_m(tot)]}\left\{1 + \frac{\beta_2}{\beta_1}\frac{[A_MB]}{[A_M]}\right\} \tag{11}$$

Using eqn. (7), eqn. (11) may be simplified as follows:

$$D=\frac{x[A_M(tot)]}{y[A_m(tot)]}+\frac{x[A_MB]}{y[A_m(tot)]}\left(\frac{\beta_2}{\beta_1}-1\right) \tag{12}$$

The first term in eqn. (12) is the cocrystallization coefficient determined in the presence of a complex former (D_{pr}). Using eqns. (3) and (10), eqn. (12) may be transformed as follows:

$$D_{pr}=D\frac{[1+([A_MB]/[A_M])]}{[1+(\beta_2[A_MB]/\beta_1[A_M])]} \tag{13}$$

where D is the cocrystallization coefficient in the absence of a complex former.

If $[A_M]\ll(\beta_2/\beta_1)[A_MB]$, then

$$D_{pr}\approx D\frac{\beta_1}{\beta_2} \tag{14}$$

and the practical cocrystallization coefficient reaches its limiting value. Obviously, using eqn. (14) one may solve another problem, i.e. the determination of the ratio of stability constants for complex compounds of micro- and macroelements. This ratio may be determined from eqn. (13):

$$\frac{\beta_2}{\beta_1}=\frac{1+([A_MB]/[A_M])-(D_{pr}/D)}{D_{pr}[A_MB]/D[A_M]} \tag{15}$$

If the stability constant of a complex macrocomponent compound is known, it is not difficult to determine the stability constant for a complex microelement compound.

The cocrystallization method was successfully used to determine the stability constants for the complex compounds of Eu^{2+}, Yb^{2+} and Es^{2+} with a tetraphenylborate ion, when the Sr^{2+} macrocomponent does not form complex compounds with a ligand. This problem is presented in Sect. F.(i).

So far we have considered cases of isomorphic cocrystallization not only when the composition of cocrystallizing components may be written as one general formula, but also when there is a coincidence of cation and anion charges. On the other hand, in many cases the charges of cocrystallizing cations differ, e.g. $SmCl_2$–$LaCl_3$ or NaCl–$FmCl_2$, etc. These patterns of cocrystallization are caused by heterovalent isomorphism, i.e. by the formation of anomalous mixed crystals. Since the formation of anomalous mixed crystals is related to the appearance (or existence) of Schottky defects in the cation or anion parts of the sublattice, the anomalous mixed crystals are characterized, as a rule, by the availability of the lower limit of mixing. This can be illustrated by the cocrystallization of $NpCl_3$ and $SmCl_2$ (Table 5). The presence of the lower limit of mixing is one of the specific features making

TABLE 5

Influence of ^{237}Np concentration on its cocrystallization coefficient with $SmCl_2$ [21]

^{237}Np concentration (mg ml^{-1})	Cocrystallization coefficient
Microquantity	0.46 ± 0.03
0.025	0.24 ± 0.02
0.05	0.09 ± 0.01

isomorphic cocrystallization distinguishable from the formation of anomalous mixed crystals. Another method of distinguishing between these two types of cocrystallization is as follows. Mono-, di- and trivalent ions were able to cocrystallize with the solid phase $SrI_2 \cdot 18C6$ from the solution in tetrahydrofuran.

In the general case, a heterogeneous equilibrium may be written as:

$$MI_{n(liq)} + SrI_2 \cdot 18C6_{(sol)} = MI_n \cdot 18C6_{(sol)} + SrI_{2(liq)}$$

where n is equal to 1, 2 or 3, depending on the ionic charge of the microcomponent. If dissociation of the components in the solution is assumed to be complete, then the equilibrium constant 'K' will be equal to:

$$K = \frac{x_{MI_n \cdot 18C6} f_{MI_n \cdot 18C6} [Sr^{2+}][I^-]^2 \gamma^3_{\pm SrI_2}}{y_{SrI_2 \cdot 18C6} f_{SrI_2 \cdot 18C6} [M^{n+}][I^-]^n \gamma^{n+1}_{\pm MI_n}} \tag{16}$$

where f is the activity coefficient in the solid phase and γ is the mean ionic activity coefficient in the solution.

Substituting the value of the cocrystallization coefficient D, in eqn. (16), we have [36]:

$$D = K' [I^-]^{n-2} \tag{17}$$

From this equation it follows that, based on the dependence of the cocrystallization coefficient on $[I^-]$, we can determine the charge of the ion of the cocrystallizing microcomponent.

At first Mikheev et al. [36] studied the dependence of the coefficients of cocrystallization of Na^+, K^+ and Cs^+ with $SrI_2 \cdot 18C6$ on the concentration of I^- in tetrahydrofuran. The necessary concentration of I^- in the solution was provided by introducing LiI, as Li^+ ions do not participate in cocrystallization with $SrI_2 \cdot 18C6$. As is seen in Fig. 6, the cocrystallization coefficient of Na^+, K^+ and Cs^+ depends linearly on $[I^-]^{-1}$. Hence, SrI_2 and MI are completely dissociated in tetrahydrofuran, and the ratio of the activity coefficients in the solution remains constant, with the concentration of LiI varying from 0.015 to 0.2 mol l^{-1}.

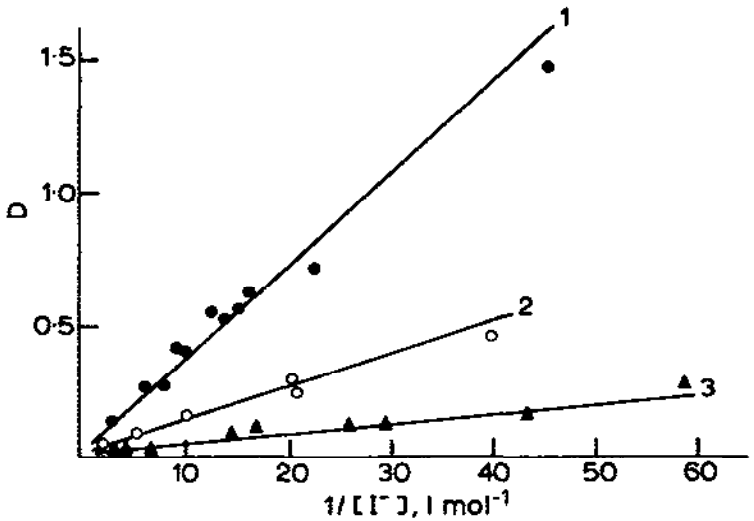

Fig. 6. Dependence of cocrystallization coefficients of Cs^+ (1), K^+ (2) and Na^+ (3) with $SrI_2 \cdot 18C6$ on $1/[I^-]$ in THF [36].

The study of cocrystallization of SmI_2, YbI_2 and EuI_2 with $SrI_2 \cdot 18C6$ showed the lack of dependence of D on the I^- concentration (Fig. 7), which points to the complete dissociation of lanthanide diiodides in a tetrahydrofuran solution.

As far as the behaviour of YI_3 is concerned, in the region of low I^- concentration, its cocrystallization coefficient does not depend on the I^- concentration, and beginning at $I^- = 0.15$ mol l^{-1}, the D value starts to decrease. The authors explain this phenomenon by the formation of the doubly charged $[YI]^{2+}$ complex at low I^- concentrations. Increasing the

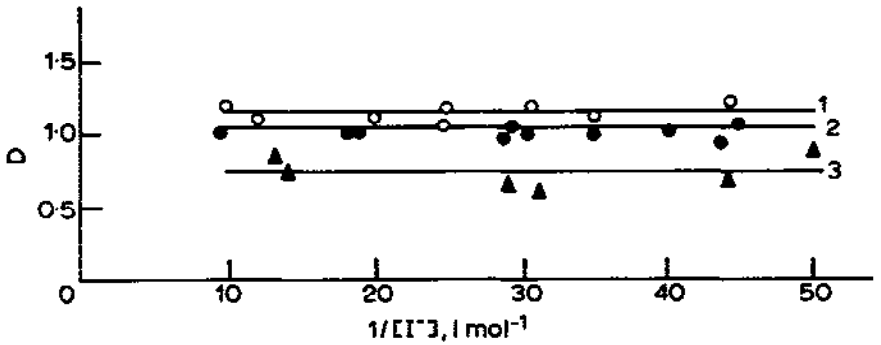

Fig. 7. Dependence of cocrystallization coefficients of Sm^{2+} (1), Eu^{2+} (2) and Yb^{2+} (3) with $SrI_2 \cdot 18C6$ on $1/[I^-]$ in THF [36].

I^- concentration causes the transition of this complex into a mono-charged one and then, obviously, into the non-crystallizing, neutral complex YI_3.

The same approach was used [37] to elucidate the oxidation state of californium, einsteinium and fermium in the presence of a strong reducer, i.e. divalent thulium. As is seen from Table 1, the oxidation potential of the couple Tm^{3+}/Tm^{2+} is considerably lower than those of Cf, Es and Fm. Hence, all these elements in the presence of Tm^{2+} are reduced quantitatively to their divalent oxidation states. However, the authors [37] considered the possibility of reducing the actinides from Cf to Fm to their monovalent states by divalent thulium. Simultaneously with the actinides, these authors studied the behaviour of Sm^{2+}, Eu^{2+} and Yb^{2+} which, like Cf, Es and Fm, reduce quantitatively to the divalent states in the presence of divalent thulium. The data obtained are listed in Figs. 7 and 8, showing that in all the elements mentioned above the coefficient of cocrystallization with $SrI_2 \cdot 18C6$ does not differ much from 1 nor depend on the I^- concentration. Thus the charges of these elements in THF solution are the same as those of strontium and equal 2+. Neither divalent lanthanides nor divalent actinides form simple complexes of the type $[MI]^-$ or MI_2 in tetrahydrofuran up to $[I^-] \approx 0.1$ mol l^{-1}. On the other hand, all these elements, due to true isomorphism with $SrI_2 \cdot 18C6$, take part in the formation of a solid solution and, consequently, form compounds of the type $MI_2 \cdot 18C6$. As has been reported [32], the same properties are characteristic of divalent americium, which, in the presence of

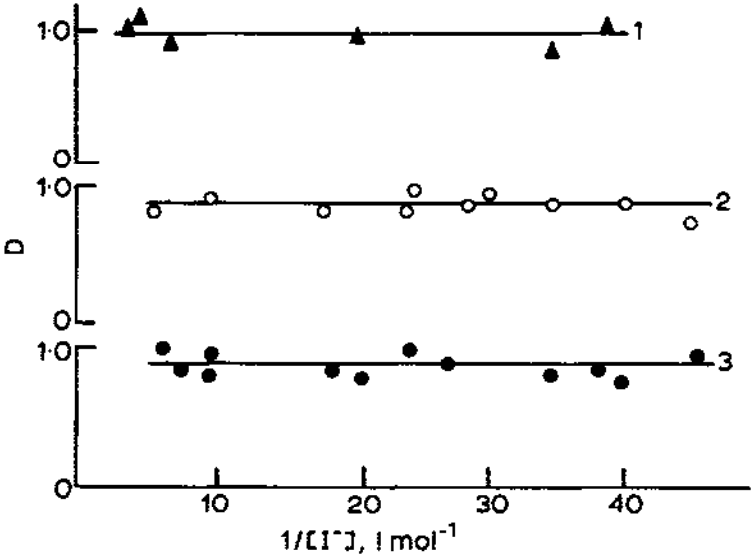

Fig. 8. Dependence of cocrystallization coefficients of Cf^{2+} (1), Es^{2+} (2) and Fm^{2+} (3) with $SrI_2 \cdot 18C6$ on $1/[I^-]$ in THF [32].

Tm^{2+}, reduces to its divalent state and, with its cocrystallization coefficient close to 1, transforms to the solid phase $SrI_2 \cdot 18C6$.

The authors used a similar approach to determine the oxidation state of Md and Fm in the presence of reducing agents as well as their ability to form chloride complexes. Studying the cocrystallization of Md and Fm with NaCl and KCl from aqueous ethanolic solutions, the authors established that, without a reducing agent, Md^{3+} and Fm^{3+} did not cocrystallize with either NaCl or KCl. However, in the presence of divalent Eu, mendelevium cocrystallized with both NaCl and KCl while Fm, remaining in its trivalent state, did not participate in cocrystallization. If Sm^{2+} is introduced as a reducing agent, fermium also takes part in cocrystallization. Based on the study of the dependence of the cocrystallization coefficient on the Cl^- concentration, the authors [38] showed that Md^{3+} reduced to its monovalent state since its cocrystallization coefficient did not depend on $[Cl^-]$. At the same time, Fm^{3+} is reduced by Sm^{2+} only to its divalent state, as the cocrystallization coefficient of Fm^{2+} increases linearly with the Cl^- concentration. These dependences also show that neither Md^+ nor Fm^{2+} form observable complexes with Cl^-. Otherwise, a departure of $D = f[Cl^-]$ from linearity to lower D values should have been observed (see Fig. 9).

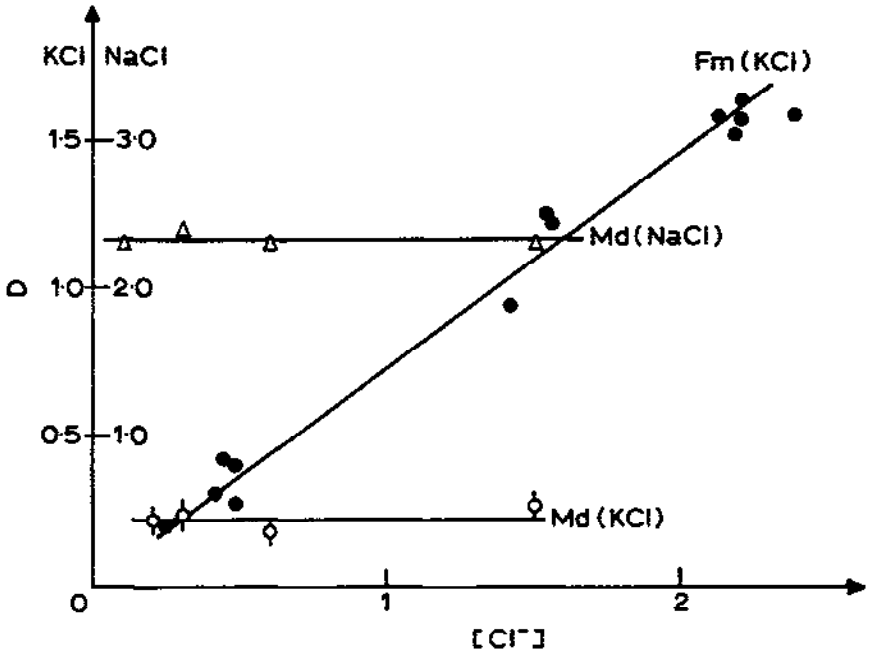

Fig. 9. Dependence of the Md^+ and Fm^{2+} cocrystallization coefficients with MCl on the chloride-ion concentration [38].

Thus, one cannot help emphasizing the effectiveness of the new approach toward studying complex compounds with the use of the cocrystallization method. In fact, this method has proven to be most suitable for studying complex compounds of radioactive elements which are present in ultramicro concentrations, especially when dealing with organic solvents.

E. HYDRATION AND SOLVATION OF THE DIVALENT LANTHANIDES AND ACTINIDES

The interaction of metal ions with water and other solvents is a problem of major importance in coordination chemistry. This also refers to the lanthanides and actinides in lower oxidation states. These issues will be considered below in Sects. E.(i) and E.(ii).

(*i*) *Hydration of* Ln^{2+} *and* An^{2+} *ions*

The hydration energy value is an important thermodynamic characteristic of the hydration process. In a simpler case, when the hydration energy is mainly determined by the ion–dipole coupling, this value may be calculated theoretically using the Born equation. However, the ion–dipole coupling is often complicated by additional factors increasing the hydration energy. These are the splitting of the *f*-, *d*- or *p*-levels of the central ion in the ligand crystalline field, the overlapping of orbitals of the central ion and *p*-, *s*-orbitals of oxygen, and many other factors. As a result, the hydration energy deviates from the value calculated according to the Born equation. Using the standard oxidation potentials for the lanthanides $E^0_{M^{3+}/M^{2+}}$ (Table 1), the energy of the third ionization stage [39], as well as the hydration energy of trivalent lanthanides [41], the authors [42] calculated the hydration energy of all the divalent lanthanides from La to Yb according to eqn. (1).

It appeared that, for most, the hydration energy increased linearly with an increase in the atomic number of the element, as in the case of Ln^{3+} (Fig. 10). The exceptions are La^{2+}, Ce^{2+}, Gd^{2+} and Tb^{2+}, elements which, in their divalent states, have an $f^{n-1}d^1$ electronic configuration. The hydration energies of these elements increase by approximately 1.5 eV, i.e. by their stabilization energy value. As for the other elements, the change in the inverse hydration energy value as a linear function of the ionic radius is in conformity with the Born equation (Fig. 11). The linear dependence embraces a series of lanthanides irrespective of their *f*–*d* excitation energy. Thus the *f*–*d* excitation energy does not affect the hydration energy of divalent lanthanides. However, the validity of this conclusion should be confirmed by comparison of the divalent lanthanides with alkaline earth elements. The hydration energy of alkaline earth elements was obtained by Mikheev and Rumer [42] from the enthalpy and entropy of hydration determined by other scientists. The hydra-

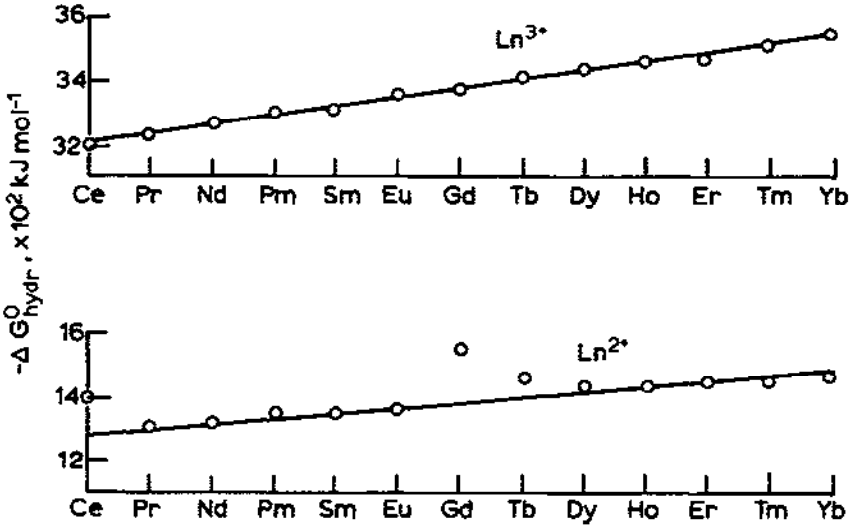

Fig. 10. Hydration energies of the divalent and trivalent lanthanides [47].

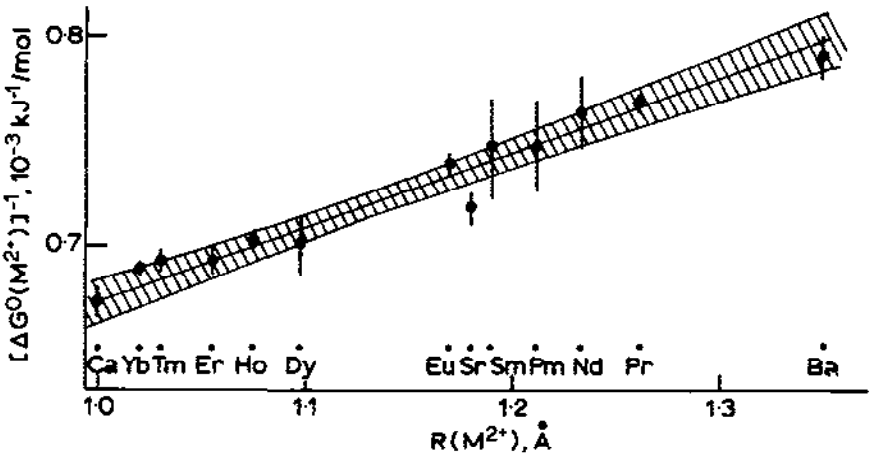

Fig. 11. Dependence of the hydration energy of divalent elements on the ionic radius [20].

tion energy values lie in a straight line, reflecting the change in the Ln^{2+} hydration energy, according to the Born equation [42]. These results undoubtedly reflect a profound similarity between the divalent lanthanides having an $f^n d^0$ configuration, and the alkaline earth elements.

In addition to the experimental determination of the Ln^{2+} hydration energy [42], David [43] calculated theoretically the enthalpies and entropies of these elements in the oxidation state 2+. It appeared that the absolute hydration energy values differed by 100–150 kJ mol^{-1} from the values re-

ported in ref. 42, though the total character of their dependence on the increase in the atomic number remained the same except for the elements with an $f^{n-1}d^1$ configuration (Fig. 11).

Experimental data for the hydration energies of An^{2+} are not yet available. For U^{2+}, Np^{2+}, Pu^{2+} and Cm^{2+} which, in the condensed phase, have an $f^{n-1}d^1$ configuration [20], the experimental $\Delta G^0_{hydr.}$ values should differ from the theoretical linear dependence (Fig. 12) by the value of stabilization energy; for An^{2+} this is equal to ≈ 2 eV.

Thus, the experimental data and theoretical calculations lead to the conclusion that divalent lanthanides and actinides with an $f^n d^0$ configuration are the closest analogues of alkaline earth metal ions, while for elements with an $f^{n-1}d^1$ configuration, certain differences must be observed.

(ii) Solvation–hydration interaction between Eu^{2+}, Yb^{2+}, Es^{2+} and aqueous-ethanolic solutions

As was mentioned earlier, the stability of the divalent lanthanides and actinides in organic solvents is higher than in aqueous solutions. Mikheev et

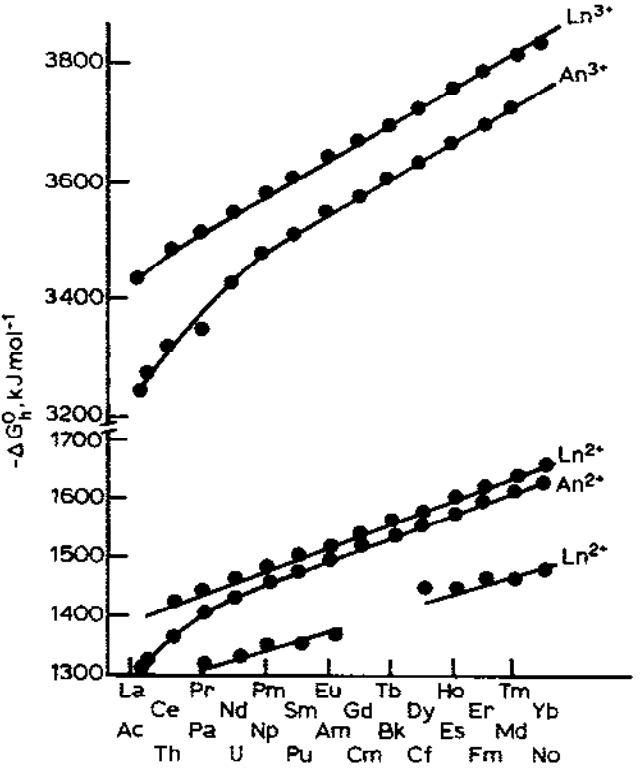

Fig. 12. Hydration energies of the di- and trivalent lanthanides and actinides [47].

al. [44] studied the solvation–hydration interaction between the divalent lanthanides and aqueous-ethanolic solutions of variable composition. They could have solved this problem by measuring the solvation–hydration energy of the ions in question. However, this is rather difficult. Instead, they determined the change in the ratio of solubility products of some salts (e.g. sulphates of macro- and microelements) while changing the composition of the solution. Since the composition of the solid phase remained constant in all the experiments, the change in the ratio of solubility products of the components took place primarily because of the change in the ratio of their solvation–hydration energies. The experimental procedure is described in detail in ref. 44.

Figure 13 shows the change in the coefficients of cocrystallization of Eu^{2+} and Yb^{2+} with the solid phase $Sr(Sm)SO_4$ as a function of water concentration in ethanol. Since

$$D = \frac{(SP)_M}{(SP)_m} K \tag{18}$$

the change in D corresponds to the change in the ratios of the solubility products of $SrSO_4$ and $LnSO_4$. As is shown in Fig. 13, with the concentration of water changing from 2 to 6 mol l^{-1}, the cocrystallization coefficient of ytterbium decreases. Hence, within this water concentration range, the SP of $YbSO_4$ increases more intensively than that of $SrSO_4$. For $EuSO_4$, the process is reversed. Obviously, the change in the water concentration leads to a rearrangement of the coordination sphere, where alcohol molecules are replaced by water. As a result, the solubility product of $YbSO_4$ increases and

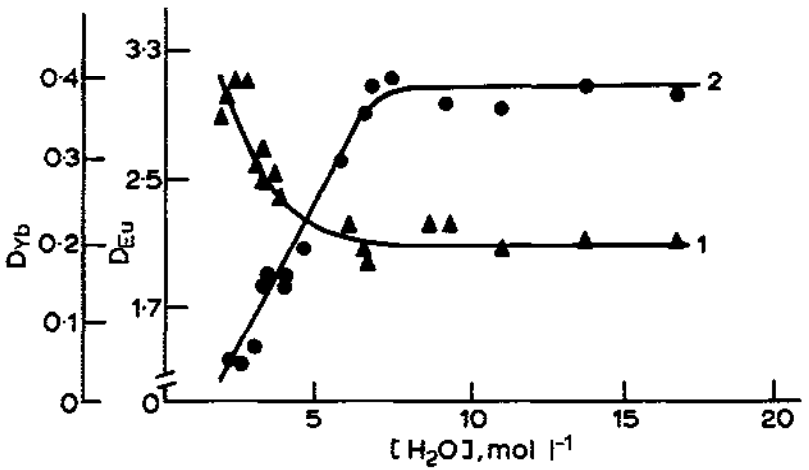

Fig. 13. Dependence of cocrystallization coefficients of Yb^{2+} (1) and Eu^{2+} (2) with $Sr(Sm)SO_4$ on $[H_2O]$ in aqueous-ethanolic solutions [44].

the solubility product of $EuSO_4$ decreases compared with that of $SrSO_4$. Therefore, the difference in the solvation–hydration energies for Yb^{2+}, Sr^{2+} and Eu^{2+} increase with increasing water concentration. For pure water, these values are shown in Table 6. An effect of increasing the solubility of $SrSO_4$ with increasing water concentration is shown in Fig. 14. Across the H_2O concentration range 2–16 mol l^{-1}, these dependences may be approximated by a straight line.

Quite an unusual process is observed in the case of $EsSO_4$ (Fig. 15). The cocrystallization coefficient of $EsSO_4$ has its minimum at the molar ratio $C_2H_5OH:H_2O = 2:1$, which corresponds to a strong solvate–hydrate complex of Es^{2+}. Increasing the water concentration leads to gradual decomposition of the complex and formation of a purely hydrated Es^{2+}. At water concentration levels exceeding 6 mol l^{-1}, the cocrystallization coefficients of $YbSO_4$

TABLE 6

Hydration energies of the divalent elements [47]

Ion	$-\Delta G^0_{hydr}$ (kJ mol^{-1})
Sr^{2+}	1401
Yb^{2+}	1461
Eu^{2+}	1361

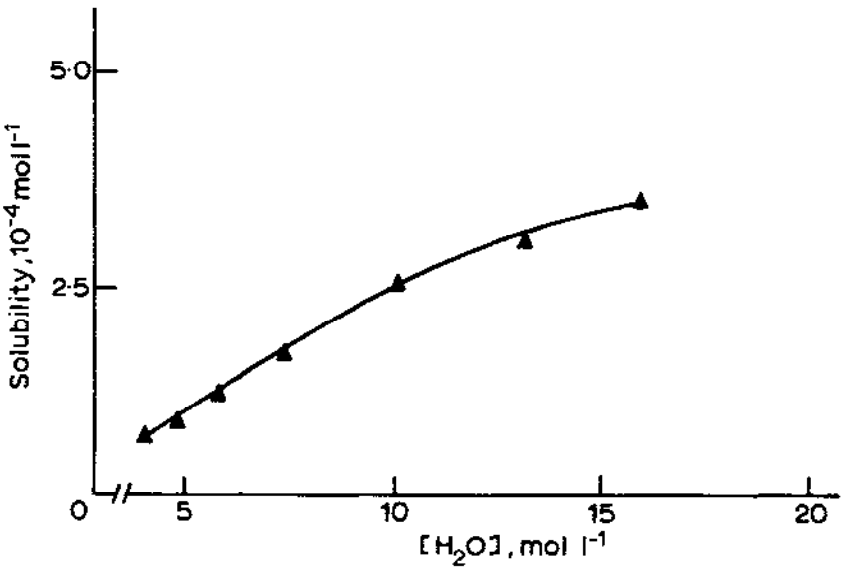

Fig. 14. Solubility of $SrSO_4$ in aqueous-ethanolic solutions [44].

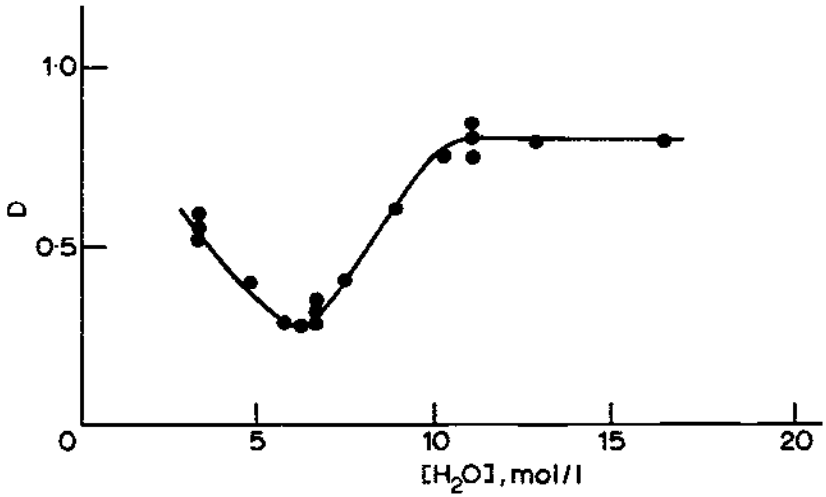

Fig. 15. Dependence of the Es^{2+} cocrystallization coefficient with $Sr(Sm)SO_4$ on $[H_2O]$ in aqueous-ethanolic solutions [44].

and $EuSO_4$ do not change. Hence, the variations of the dependences of the solubility of $YbSO_4$, $EuSO_4$ and $SrSO_4$ upon water concentration are the same for these elements. Obviously, at water concentrations of 6 mol l^{-1} and over, the coordination spheres of Eu^{2+}, Yb^{2+} and Sr^{2+} contain only water molecules. This conclusion is confirmed by spectroscopic studies, which showed that the absorption spectrum of SmI_2 in an ethanolic solution containing 10 mol l^{-1} of water coincides completely with its spectrum in pure water. Decreasing the water concentration to 5 mol l^{-1} leads to a decrease in the crystal field splitting parameter Δ, the minimum value of which is achieved in pure ethanol (Table 7). In the case of Es^{2+}, complete substitution of water for ethanol takes place only at water concentrations exceeding 10 mol l^{-1} due to the growing stability of its hydrate–solvate complexes.

The anomalous behaviour of Es^{2+} cannot be explained within the framework of existing concepts and it should be considered in further studies.

TABLE 7

Influence of the water concentration on the energy parameters of the *fd*-configuration of Sm^{2+} (10^3 cm^{-1}) [47]

Solvent	Δ	E_{fd}
H_2O	14.14	24.83
C_2H_5OH–10 mol l^{-1} H_2O	14.17	24.84
C_2H_5OH–5 mol l^{-1} H_2O	14.03	25.03
C_2H_5OH	13.46	24.45

(iii) Complex formation of the lanthanides and actinides in their lower oxidation states with halide ions

Though lanthanides in their divalent state have been known since the beginning of the 20th century, data on their interaction with halide ions in solution were not reported until the 1970s. This is explained by the then limited availability of the dihalides of these elements and also by the fact that, at that time, because of the extreme instability of Ln^{2+}, no adequate physico-chemical method existed. Attempts to use the spectrophotometric method for studying Ln^{2+}, which is most suitable for unstable systems, were unsuccessful because broad intense *fd*-transitions exist in the absorption spectra of Ln^{2+}, making the interpretation of the spectra difficult. The method proposed by Johnson and Sandoe for the interpretation of the spectra of *fd*-transitions of Ln^{2+} in a crystalline matrix [4] stimulated, as was mentioned above, studies on the properties of Ln^{2+} and U^{3+} in solution [5,6,45–48]. The use of the $J_1\gamma$-interaction scheme, as proposed by these authors for the interpretation of the absorption spectra of Ln^{2+} and U^{3+}, is complicated by a lack of information on the symmetry of the ion surroundings. However, the assumptions made by these authors [5,6,45–48], which introduce an insignificant error in the E_{fd} value (within 0.1 Δ), allow one to draw conclusions regarding the coordination properties of the elements in question.

Table 8 shows the values of energy parameters of a number of Ln^{2+} and U^{3+} halides for different solvents depending on the halide ion. From these data it follows that, in aqueous solution, neither Ln^{2+} nor U^{3+} interact with halide ions since the Δ values are the same for Cl^-, Br^- and I^-, i.e. in aqueous solutions the first coordination sphere of these elements contains only water molecules.

In organic solvents, Ln^{2+} [6] and U^{3+} [48] display their complex formation properties toward halide ions. Thus, beginning with ethanol, the absorption spectrum of Yb^{2+} changes with increasing Cl^- concentration (Fig. 16); the Δ parameter increases and the E_{fd} value decreases (Table 9). Thus, the Cl^- enters into the inner coordination sphere of the complex [49]. Table 8 shows that, in the case of Yb^{2+}, Sm^{2+} and U^{3+} present in ethanol, the Δ parameter changes, depending on the halide ion, in the order $Cl > Br > I$. A similar variation in the stability of the complexes is observed in HMPA and CH_3CN. However, in THF and PC, Δ increases with increasing size of the halide ion for all the elements in question. Thus, for U^{3+} and Ln^{2+} in solutions of HMPA, CH_3CN and C_2H_5OH, a normal spectroscopic variation of the decrease in the stability of the complexes ($Cl^- > Br^- > I^-$) is observed while in PC and THF an inverse variation ($I^- > Br^- > Cl^-$) is observed, the latter corresponding to the normal nephelauxetic variation. At present these processes are difficult to explain. Obviously, it is not only the nature

TABLE 8

Energy parameters for divalent lanthanides and uranium(III) halides in different solvents (10^3 cm^{-1}) [6,47,48]

M	X^-	H_2O		C_2H_5OH		PC		CH_3CN		THF		HMPA		E_{fd} (ref. 22)
		Δ	E_{fd}	Δ	E_{fd}	Δ	E_{fd}	Δ	E_{fd}	Δ	E_{fd}	Δ	E_{fd}	
Eu^{2+}	Cl	9.4	35.9									8.0	33.8	
	Br	9.4										7.1	32.5	34.6
	I	9.4		7.1	32.2			6.9	31.5	11.2	34.9			
Sm^{2+}	Cl	14.1	24.8							11.2	23.4	12.7	26.2	
	Br	14.1	24.8	13.7	24.5	11.2	24.0			11.5	23.3	11.4	25.4	23.5
	I	14.1	24.8	13.5	24.4	11.6	24.2	12.5	21.2	11.7	22.6	10.8	24.6	
Yb^{2+}	Cl	12.4	34.7	13.7	34.1					12.7	33.2	11.9	33.8	
	Br	12.4	34.7	12.9	33.8	12.1	33.1			13.2	32.9			33.8
	I			10.7	32.8	12.3	33.6	11.2	28.6	13.4	32.6			
Tm^{2+}	Cl									14.8	25.7			
	Br									15.3	25.4	16.0	28.1	23.1
	I									15.8	25.1			
Dy^{2+}	I									7.4	17.2			17.5
Nd^{2+}	I									6.9	11.6			13.9
U^{3+}	Cl	15.38	23.85	15.91	23.11					15.37	25.54	18.75	27.22	
	Br	15.38	23.85	15.40	23.85	12.60	23.11	14.45	24.73	16.56	26.20	14.15	25.07	27.10
	I	15.38	23.85	14.90	23.08	13.88	22.85	12.40	22.73	18.03	25.52	13.10	24.70	

TABLE 9

Energy parameters for Yb^{2+} in 96% ethanol (10^3 cm^{-1}) [47]

$[Cl^-]$ (mol l^{-1})	Δ	E_{fd}
0.04	13.6	34.2
0.06	13.8	33.8
1.6	14.0	33.6
4.0	14.2	33.4

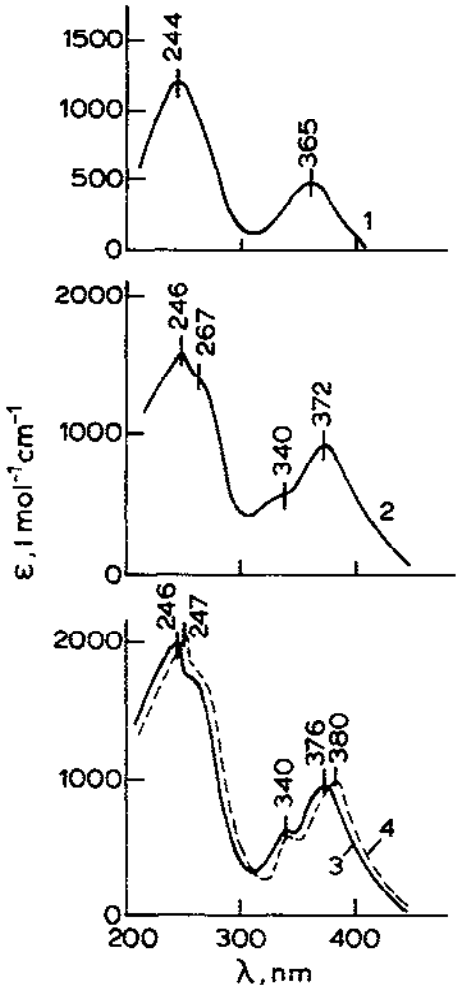

Fig. 16. The Yb^{2+} absorption spectra of *fd*-transitions in 96% C_2H_5OH. $[Cl^-]$ (mol l^{-1}): 1, 0.04; 2, 0.06; 3, 1.6; 4, 4.0 [47].

of the solvent, its dielectric constant and donor–acceptor properties, but also the changes in the coordination sphere of the ions which play an important role.

The dependence of Δ on the type of solvent shows that the solvent molecules enter into the inner coordination sphere of halide complexes of Ln^{2+} and U^{3+}. Thus, for SmI_2, Δ changes in the order $H_2O > C_2H_5OH > CH_3CN > THF > PC > HMPA$. However, this order is somewhat changed for other dihalides (e.g. Yb^{2+}), probably due to change in the coordination sphere as a result of the differences in ionic radii of Ln^{2+} and their effective charges. This is confirmed by the composition of the

products obtained in THF during the reduction of $LnCl_3$ by metallic lithium [50]. Thus, for samarium and europium, non-solvated dihalides of $SmCl_2$ and $EuCl_2$ are obtained, while for ytterbium, the compound $YbCl_2 \cdot THF$ is formed.

THF is the most suitable solvent from the point of view of stability of lower oxidation states of the elements. Besides solutions of Eu^{2+}, Yb^{2+}, Sm^{2+} and U^{3+}, stable solutions of Tm^{2+} as well as those of dysprosium and neodymium diiodides with the half-oxidation periods ≈ 0.5 and 0.34 h, respectively (Table 10) [51] were obtained in THF. Figures 17–19 show the absorption spectra of *fd*-transitions of Ln^{2+} and U^{3+} in this solution. However, from the point of view of coordination chemistry, this solvent is difficult to work with. The difficulty relates to the low dielectric constant, which results in the poor solubility in THF of chloride and bromide compounds and the formation in the solution of ion pairs and various forms of complex.

Another solvent, HMPA, which may be used at oxidation potentials up to -3.3 V, has strong solvating properties, resulting in stabilization of an element in the higher oxidation state. The ionic radius of the halide ion determining the coordination sphere of the metal ions also plays an important role. For example, in chloride solutions, Tm^{3+} is not reduced to Tm^{2+} by the solution of metallic sodium in HMPA, while in bromide and iodide solutions, reduction does take place [52].

This is accounted for by the fact, that, in contrast to chloride complexes, in the bromide complex $[TmBr_2 \cdot 4HMPA]Br$ [53] reduction of thulium to its divalent state is unrelated to the rearrangement of the inner sphere.

The role of the solvent in the stabilization of the lower oxidation state is manifested, for instance, in SmI_2 solutions in CH_3CN. These solutions are stable in the absence of traces of oxidizers. However, an attempt to obtain from them a diiodide solvate through distillation of the solvent resulted in the oxidation of Sm^{2+}.

TABLE 10

Half-oxidation periods ($T_{1/2}$) of Ln^{2+} in different solvents [47,51]

Ln^{2+}	$T_{1/2}$ (h)			
	THF	HMFA	CH_3CN	PC
Eu	Stable	Stable	Stable	Stable
Yb	Stable	Stable	Stable	Stable
Sm	Stable	~64	>270	>200
Tm	~250	~5		
Dy	~0.5			
Nd	~0.3			

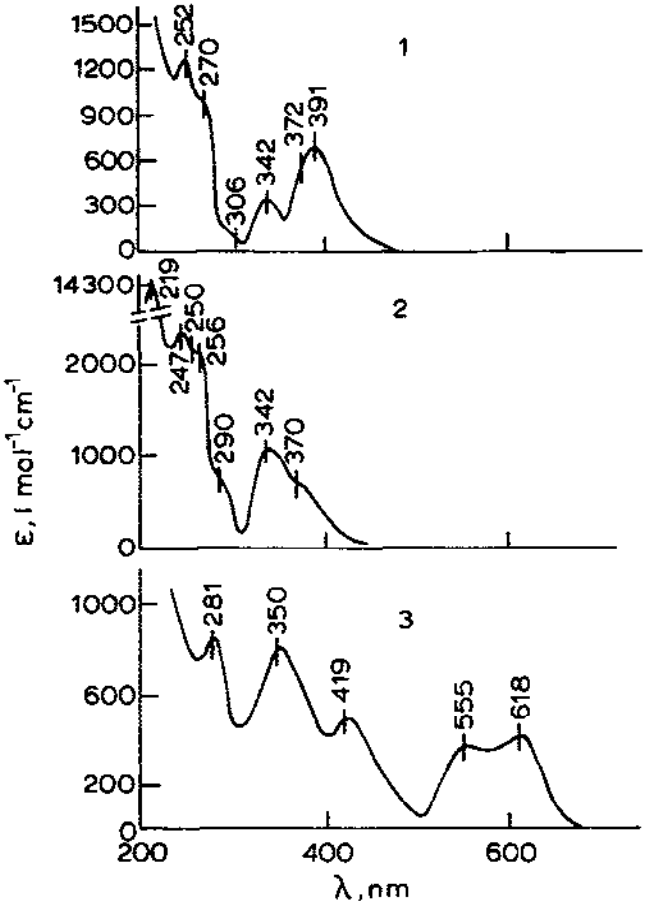

Fig. 17. Absorption spectra of *fd*-transitions of YbI_2 (1), EuI_2 (2) and SmI_2 (3) in THF [47].

Studies of the complex formation of the far actinides with the halide ion are much more difficult because weighable quantities of these elements are not suitable for work in solutions due to strong radiation effects.

Using the cocrystallization method, it was established that divalent fermium and einsteinium did not form strong chloride complexes in aqueous-ethanolic solutions [54], the same being true of univalent mendelevium [38]. In contrast to these data, in THF one can expect the formation of monocharged complexes of the type $[MHal]^+$ (where Hal represents Cl^- or Br^-) by divalent Ln and An. A similar process takes place in the case of strontium halides, whose ionic radius and properties are close to those of Ln^{2+} and An^{2+} [36].

Since all the divalent lanthanides are characterized by the presence of *fd*-

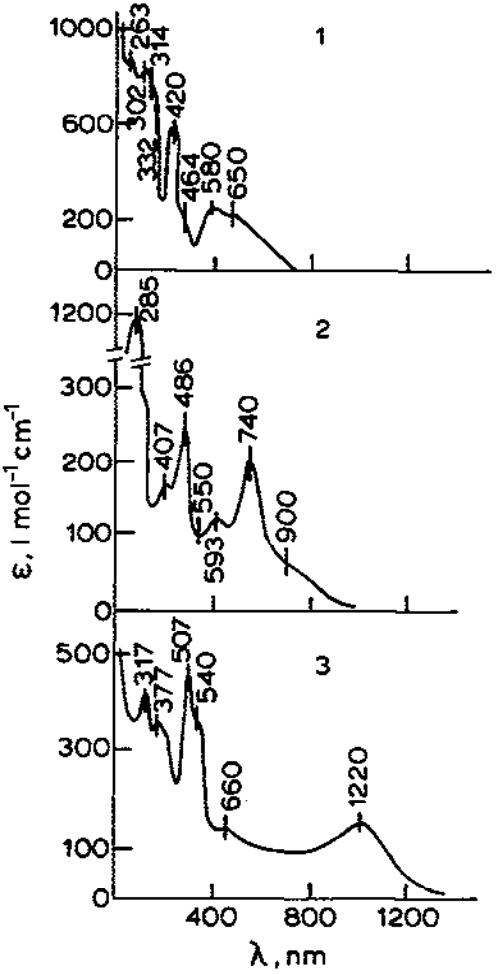

Fig. 18. Absorption spectra of *fd*-transitions of TmI_2 (1), DyI_2 (2) and NdI_2 (3) in THF [47].

transitions, it was interesting to study the influence of E_{fd} on the complex formation properties of these elements. To this end, the energy data obtained for Ln^{2+} solutions in THF (Table 8) were used. As shown in Fig. 20, the Δ value achieves limiting values for both halves of the lanthanide series. For the first half it is equal to $\approx 11.0 \times 10^3\ cm^{-1}$, and for the second half $\approx 14 \times 10^3\ cm^{-1}$ [55]. A similar dependence was obtained in ref. 4 for Ln^{2+} in the CaF_2 matrix. The only difference is that Δ for the first half of the lanthanides stays higher than that for the second half. This dependence requires further theoretical interpretation.

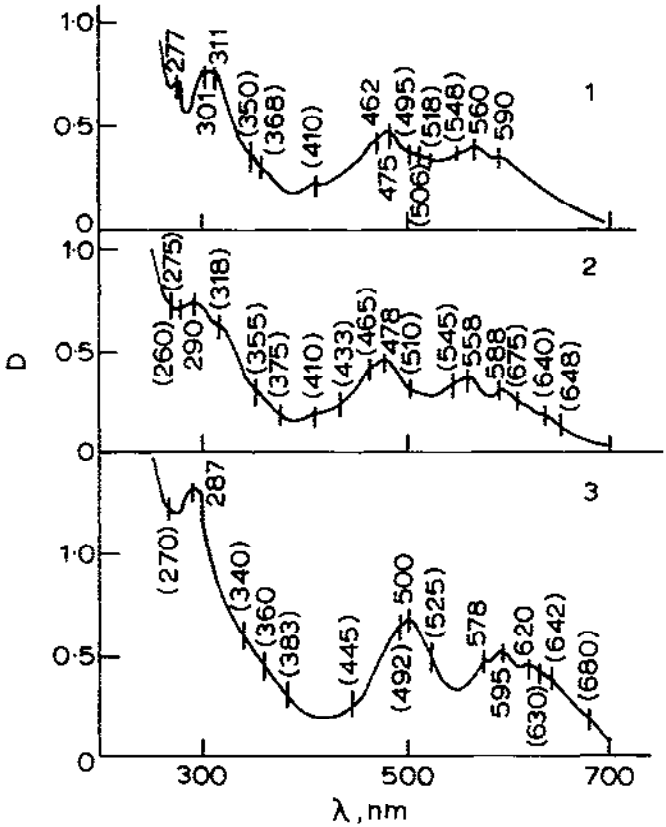

Fig. 19. Absorption spectra of $UI_3 + LiCl$ (1), UBr_3 (2) and UI_3 (3) in THF [48].

F. COORDINATION COMPOUNDS OF THE LANTHANIDES AND ACTINIDES IN THEIR LOWER OXIDATION STATES WITH ORGANIC LIGANDS

Since the lanthanides and actinides are very strong reducing agents in their lower oxidation states, the ligands involved in complex formation must be stable toward oxidation potentials up to -2.5 V. It is well known that oxyacids and carbonic acids oxidize the divalent lanthanides. As mentioned in Sect. A, the constants of complex formation with complexons were obtained only for Eu^{2+}, while the results obtained for Yb^{2+} are of qualitative character [11]. In refs. 49 and 56, it was shown that such ligands as the tetraphenylborate ion and crown ethers were stable up to an oxidation potential equal to that of the Tm^{3+}/Tm^{2+} couple, i.e. ≈ 2.3 V. Thus, complex formation of Ln^{2+} and U^{3+} with these ligands were studied.

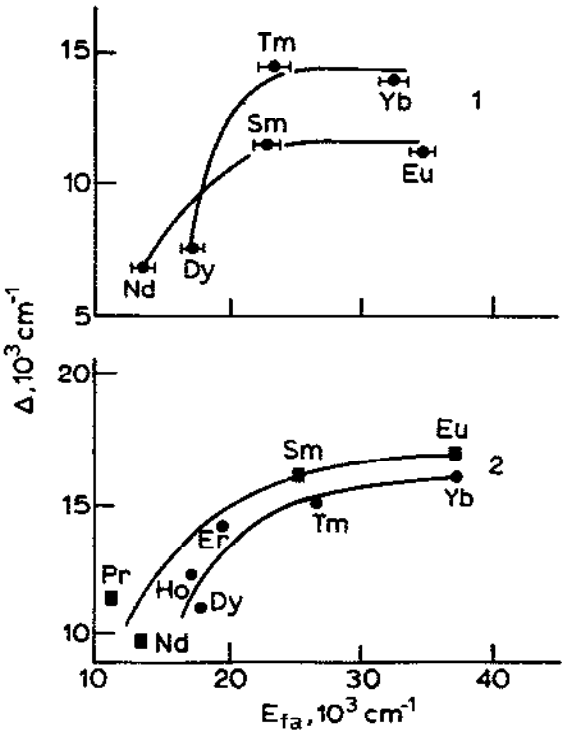

Fig. 20. Dependence of the crystal field splitting parameters (Δ) on E_{fa} in THF (1) and CaF_2 (2) [47].

(i) Complex formation of Eu^{2+}, Yb^{2+} and Es^{2+} with the tetraphenylborate ion

It is well known that TPB^-, due to its large dimensions and low charge, does not tend to form complexes. In this respect, the considerable stabilization of aqueous solutions of Yb^{2+} and Sm^{2+} in the presence of sodium tetraphenylborate were unexpected. Studies on the dependence of the oxidation kinetics of Sm^{2+} in water with TPB^- concentration (Table 11) showed that increasing NaTPB concentration up to 0.08 mol l^{-1} led to a 50-fold decrease in oxidation rate (and correspondingly to an increase in the half-oxidation period, $T_{1/2}$) of Sm^{2+} compared with a pure water solution.

The stabilization of aqueous solutions of Sm^{2+} and Yb^{2+} in the presence of NaTPB may be due to several factors. These include a change in the water structure in the presence of large anions, a decrease in the activity coefficients of the ions with an increase in the ionic force of the solution, plus formation by divalent lanthanides of complexes with the TPB ion, resulting in stabilization due to the 'umbrella effect', which helps to isolate the ion from contact with the oxidizing agents present in the medium. The influence of the first

TABLE 11

Reaction constants for the oxidation and the corresponding half-oxidation periods of Sm^{2+} in water [49]
$[Sm^{+}] = 0.02$ mol l^{-1}.

$[Sm^{2+}]$:[TPB]	K^a (10^{-6} s^{-1})	$T_{1/2}{}^b$ (h)
Without TPB	60.0	3
1:1	20.0	10
1:2	17.0	11
1:3	4.0	46
1:4	1.2	160
1:5	1.4	143
1:6	1.6	121

[a] K = oxidation rate constant.
[b] $T_{1/2}$ = half-oxidation period.

two factors may be excluded if we take into account data for experiments with $NaClO_4$ in aqueous solutions of Sm^{2+}. The perchlorate ion, at the same concentrations as TPB^-, did not have a marked effect on the stabilization of Sm^{2+} in aqueous solutions.

Thus, in this case we can only speak about the formation of Sm^{2+} complexes with the TPB ion. However, the absorption spectra, which should be sensitive to the presence of NaTPB, were fully identical with those of Sm^{2+} in water [57]. This implies that the inner coordination sphere of Sm^{2+} is saturated with water molecules, and no direct interaction between Sm^{2+} and TPB^- takes place. Therefore, in this case we can presume the formation of outer-sphere complexes [58]. The feasibility of formation of such complexes by the divalent lanthanides and actinides was demonstrated by Eu^{2+}, Yb^{2+} and Es^{2+} in aqueous-ethanolic solutions with a water concentration of 10 mol l^{-1} [59]. At this level of water concentration, the immediate surroundings of Ln^{2+} are the same as in pure water, a fact determined using the spectrophotometric technique [57]. To determine the composition of the complexes and their stability constants, the cocrystallization method of microquantities of Eu^{2+}, Yb^{2+} and Es^{2+} with a solid $Sr(Sm)SO_4$ solution was used [59]. The presence of Sm^{2+} was necessary to maintain the oxidation potential of the system. The samarium content in the solid phase was constant and equal to $\approx$10 mol.%.

In the case of the monovalent TPB ion and with the condition that the strontium macrocomponent does not form complexes with the TPB ion

$$\frac{D_0}{D} = 1 + K_1 L + \ldots + K_n L^n \tag{19}$$

where D and D_0 are the cocrystallization coefficients in the presence and absence of a ligand, respectively, K_n are the complex formation constants, and L is the ligand concentration. Thus, by studying the dependence of D on the ligand concentration we can determine the K values.

First of all, it was shown that Sr^{2+} did not actually form complexes with the TPB ion. This conclusion was based on the fact that the solubility of $SrSO_4$ in aqueous-ethanolic solutions showed no dependence on the NaTPB concentration [59]. Besides, using ion-exchange resins only cation and neutral complexes were formed in the system studied while anion complexes were not observed. Hence, eqn. (19) may be written:

$$\frac{D_0}{D} = 1 + K_1 L + K_2 L^2 \tag{20}$$

Figure 21 shows the dependence of D for Eu^{2+}, Yb^{2+} and Es^{2+} on $[TPB^-]$ in solution. To calculate the K_1 and K_2 values for the complexes in question, a curve approximation program for the equation with one and two ligands was used. The values of K_1 and K_2 obtained are listed in Table 12. K_2 is higher than K_1 by 1–2 orders, i.e. the formation of complexes with two ligands is much more likely. At the same time, the K_1 and K_2 values are not large. K_2 values for europium and ytterbium parallel the hydration energy values for these elements and the dimensions of their hydration ions, i.e. $K_{Eu^{2+}} > K_{Yb^{2+}}$. The K_1 value for Es^{2+} is 2–4 times higher than those for Eu^{2+} and Yb^{2+}. In other words, we can assume that the dimensions of the hydrated Es^{2+} ion are smaller than those of Eu^{2+}. This is in accord with the ability of Es^{2+}, unlike Eu^{2+}, to cocrystallize with KCl and NaCl in aqueous-ethanolic solutions [60,61]. On the other hand, an effect of complex formation with TPB ion is observed for Ln^{2+} and An^{2+}, but not for Sr^{2+}.

It can be assumed that *f*-electrons play a role in the complex formation of Ln^{2+}. In this case, trivalent lanthanides also must yield complexes with TPB ions. However, studies on the solubility of $Yb_2(SO_4)_3$ in aqueous-ethanolic solution showed that the influence of NaTPB on the solubility ($\approx 1.4 \times 10^{-3}$ mol l^{-1}) remains constant up to the concentration of NaTPB = 0.3 mol l^{-1}, i.e. complex formation of Yb^{3+} with the TPB ion did not take place.

It was assumed that the outer-sphere interaction with TPB^-, characteristic of Eu^{2+}, Yb^{2+} and Es^{2+}, was due to some delocalization of the electron involving the participation of phenyl groups of TPB ions. This may occur because of electron tunnelling through the hydrate shell of the ion. In the case of Es^{2+}, this effect must be stronger due to the smaller dimensions of its hydrate shell. This may become an additional factor causing the stabilization of Es^{2+} complexes with the TPB ion.

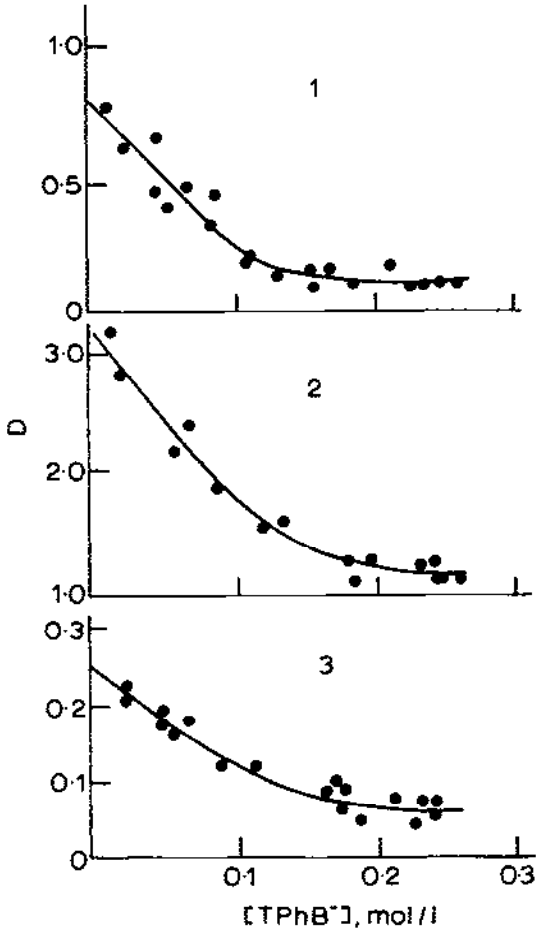

Fig. 21. Dependence of the cocrystallization coefficients of Yb^{2+} (1), Eu^{2+} (2) and Es^{2+} (3) with $Sr(Sm)SO_4$ on TPB^- concentration [59].

TABLE 12

Complex formation constants for Ln^{2+} with TPB in C_2H_5OH 10 mol l^{-1} H_2O [59]

M^{2+}	K_1[a]	K_2[b]
Yb	6.5 ± 0.5	25.7 ± 1.1
Eu	1.7 ± 0.4	52.7 ± 2.3
Es	6.2 ± 0.5	106.4 ± 2.2

[a] K_1 (l mol^{-1}) = the first stability constant.
[b] K_2 (l^2 mol^{-2}) = the second stability constant.

Based on the above results, we conclude that the complexes $[M(H_2O)_n]$ TPB_2, where M is Yb^{2+}, Eu^{2+}, Es^{2+}, were formed.

Obviously, a similar charge transfer is responsible for the formation of stronger complexes of Eu^{2+} (compared with those of Eu^{3+} and Sr^{2+}) with *o*-phenanthroline, bipyridine, tripyridintriarsine, having non-saturated bonds. The strength of the Eu^{2+} complexes increases in the order TPTA > *o*-phen > bipyridine [62].

The uranium(III) ion, which, like the divalent lanthanides, also possesses the ability to transfer electron density to the ligand, is a strong reducing agent. Therefore one can expect it to interact with the TPB ion. This interaction leads to the stabilization of aqueous solutions of U^{3+}. The study of the U^{3+} oxidation kinetics in aqueous solutions ($[U^{3+}] = 1.5 \times 10^2$ mol l^{-1}) showed that the presence of TPB ions in the solution at a concentration of 0.06 mol l^{-1} led to a tenfold increase in the stability of the solution.

At the same time, studies on the possibility of using the TPB ion in organic solvents at oxidation potentials below that of the Tm^{3+}/Tm^{2+} couple showed that divalent Dy and Nd were immediately oxidized by this ligand [56].

(ii) Complex formation of lanthanides and actinides in their lower oxidation states with neutral macrocyclic polyethers

Macrocyclic polyethers, and particularly crown ethers and cryptands, are rather stable to low oxidation potentials. For instance, the alkali metal anions Cs^-, K^- and Na^- were obtained in THF solution in their presence [63]. Complexes of divalent dysprosium and neodymium with 18C6 (see Sect. F) were obtained from solutions in this solvent. Therefore these ligands attracted the attention of research workers involved in studying lower oxidation states of Ln and An with a view to stabilizing them in solution.

(a) Complex formation of Ln^{2+} and An^{2+} with macrocyclic polyethers in solution

Recently, a number of publications concerning the problem of complex formation of Ln^{2+} and An^{2+} with crown ethers and cryptands have appeared. A detailed analysis of these results is presented in refs. 47 and 64–66. In this section, we shall consider the data of principal importance for the discussion of the problems of complex formation of Ln and An in lower oxidation states as well as data that have not yet been reported in papers [64–66].

Japanese scientists determined complex formation constants for divalent Eu, Yb, Sm [67,68], Cf [67], Am [69], Ac [70] with crown ethers in aqueous solutions using the radiopolarographic method. For Yb^{2+} with 18C6 they give complexes of two compositions: 1:1 [67] and 1:2 [68] with log β equal to 2.4 and 3.8–4.3, respectively. The samarium complex of the composition

1:2 has $\log \beta = 6.3–6.9$, and the complexes for divalent Eu, Cf, Am and Ac of the composition 1:1 are characterized by $\log \beta$ equal to 2.7, 2.0, 2.6–3.0 and 5.4–6.3, respectively.

The value $\log \beta = 2.53 \pm 0.06$ for the Eu^{2+} with 18C6 (1:1), obtained for aqueous solutions using the conductometric method [71], agreed with the data reported by Shiokawa and Suzuki [67].

Unfortunately, data for Ac^{2+}, Ac^{+} and Am^{2+} are questionable, since obtaining Ac^{2+} ($E^0_{Ac^{3+}/Ac^{2+}} = -4.9$ V) [70] and especially Ac^{+} seems incredible. The complex $TmI_2 \cdot 18C6$ is instantly oxidized in aqueous solutions, though $E^0_{Tm^{3+}/Tm^{2+}}$ is much higher (−2.3 V). The same is true of the Am^{2+} complex with crown ether because the oxidation potential of the Am^{3+}/Am^{2+} is close to that of Tm^{3+}/Tm^{2+}. It is therefore difficult to asume that the Am^{2+} complex might exist in aqueous solution. Obviously, the reason for this discrepancy should be looked for in the radiopolarographic method, which itself has been insufficiently studied [72].

Based on Ln^{2+} complex formation constants with crown ethers, one could expect that stability should increase in aqueous solution in the presence of these ligands. However, studies on the influence of crown ethers on the oxidation of Sm^{2+} solutions in water with the use of the spectrophotometric technique showed that, though some increase in the stability of Sm^{2+} solutions in the presence of 18C6 and 15C5 was observed, there was no pronounced stabilization (Table 13). This is probably due to a low value of the standard oxidation potential of the Sm^{3+}/Sm^{2+} couple (Table 1), where the kinetic parameters of the redox processes rather than the thermodynamic factors of the complex formation start to play a determining role.

From this point of view the data on the stabilization of Sm^{2+} in aqueous solution in the presence of DCH18C6 (Table 13) are of interest. This ligand has two isomers: *cis-syn-cis* and *cis-anti-cis*. Complex formation with the first

TABLE 13

Influence of crown ethers on the oxidation velocity of $SmCl_2$ in water [56] $[Sm^{2+}] = 0.01$ mol l^{-1}.

Crown ether	$[Sm^{2+}]$:[crown]	K (10^{-4} s^{-1})	$T_{1/2}$ (h)
Without crown ether		5.7	0.34
12C4	1:4	3.7	0.52
15C5	1:4	1.5	1.27
18C6	1:2	1.9	1.00
DB18C6	1:2	7.7	0.25
DCH18C6(*cis-syn-cis*)	1:2.5	0.17	11.3
DCH18C6(*cis-anti-cis*)	1:2.5	0.4	1.4

isomer leads to the envelopment of the Ln^{2+} ion with a 'pan' complex and its isolation from the environment. This results in a tenfold increase in the half-oxidation period ($T_{1/2}$) of Sm^{2+} in water.

Complex formation of Ln^{2+} with crown ethers is stronger in aqueous-organic solvents. For example, the Eu^{2+} complexes with 18C6 in ethanol containing 10 mol l^{-1} H_2O have $\log \beta = 4.72 \pm 0.13$ [71], i.e. their stability increases by more than two orders of magnitude compared with aqueous solutions.

Ln^{2+} form even stronger complexes in propylene carbonate [73,74]. Thus, for complexes with DBB18C6 of the composition 1:1, $\log \beta_{Sm^{2+}} = 7.60 \pm 0.05$ and $\log \beta_{Yb^{2+}} = 7.31 \pm 0.10$. In crown ethers with a smaller ring (12C4, BB15C5) complexes of the composition 1:2 are formed, their stabilities being by 1–2 orders higher ($\log \beta_{Sm^{2+}} = 8.4$ and 10.8, respectively, $\log \beta_{Yb^{2+}} = 8.3$ and 8.4, respectively). In PC, Ln^{2+} form strong complexes with DB30C18 ($\log \beta_{Sm^{2+}} = 8.3$, $\log \beta_{Yb^{2+}} = 7.5$). The stability of the Ln^{3+} complexes is 3–5 orders lower under the same conditions.

To follow the stabilization of Ln^{2+} in PC in the presence of crown ether, it is interesting to consider Tm^{2+} solutions [47,75]. During the dissolution of TmI_2 in PC and CH_3CN, Tm^{2+} is instantly oxidized. The complex formation of Tm^{2+} with 18C6 in these solvents resulted in Tm^{2+} solutions with half-oxidation periods ≈ 6 min in CH_3CN and 20 min in PC. The spectra of these solutions are shown in Fig. 22. In CH_3CN, the $TmI_2 \cdot 18C6$

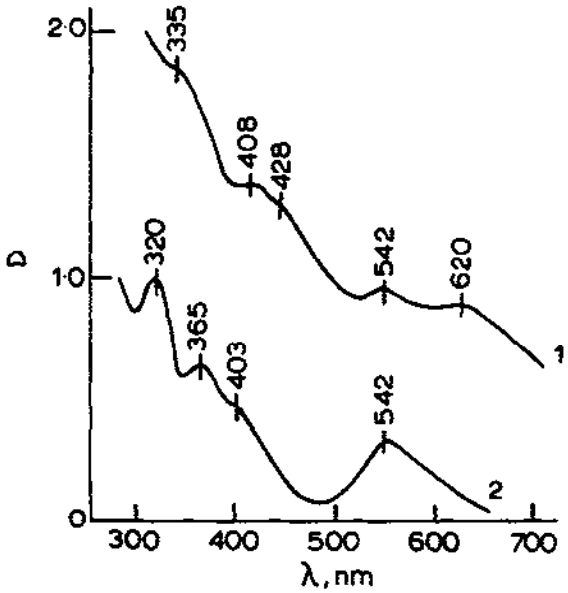

Fig. 22. Absorption spectra of $TmI_2 \cdot 18C6$ in CH_3CN(1) and PC(2) [47].

solutions are light green and in PC they are red. An analogous change in the colour was also observed in the case of $SmI_2 \cdot 18C6$ from CH_3CN to PC. At the same time, solid complexes of these elements obtained from THF solutions are blue-green and blue for Tm^{2+} and Sm^{2+}, respectively (see Sect. G.(i)). Hence, in these solutions, the solvent molecules take part in coordination with $[Ln \cdot 18C6]I_2$ and affect the spectral characteristics of the solutions of these elements according to their donor–acceptor properties. This follows from the data in Table 14 where values of the energy parameters of Ln^{2+}, obtained using the $J_1\gamma$-interaction scheme, are reported. Table 14 also contains data on the complex formation of Ln^{2+} with oxygen- and sulphur-containing crown ethers. As shown in Table 12, the energy of the unsplit level of the *fd*-configuration (E_{fd}) is close to that reported elsewhere for other solvents and free ions [6,22]. The crystal field splitting parameter (Δ) for one and the same solvent depends on the anion and the crown ether and decreases in passing from pure solvent to solutions containing crown ethers in the order solvent > DT18C6 > 18C6, i.e. the strongest lanthanide–anion interaction occurs in pure solvent. This phenomenon is explained by the screening effect of the crown ether ring and higher electronegativity of oxygen compared with sulphur, which contributes to a decrease in the electrostatic intensity of the crystal field of the complexes with 18C6 compared with DT18C6.

Since the presence of oxygen and sulphur-containing crown ethers results in a slight change in the energy parameters of Ln^{2+} in solution, it can be concluded that Ln^{2+} forms complexes with both polyethers due to the ion–

TABLE 14

Energy parameters for Ln^{2+} in different media (10^3 cm^{-1}) [47]

$[Ln^{2+}]$ (mol l^{-1})	Solvent	Anion	Δ			E_{fd}			E_{fd} (ref. 22)
			Without crown ether	DT18C6	18C6	Without crown ether	DT18C6	18C6	
Eu^{2+}	CH_3CN	I^-	6.97	6.79	6.64	31.47	31.08	31.05	34.60
(0.066)	PC	I^-		8.42	7.27		32.47	31.45	
Yb^{2+}	CH_3CN	I^-	11.44	10.44	9.78	28.63	30.78	31.21	
(0.015)	PC	I^-	12.33			33.64			33.80
	PC	Br^-	12.15	12.00	11.93	33.98	34.98	34.55	
Sm^{2+}	CH_3CN	I^-	12.47	11.60	11.40	21.15	21.90	22.90	
(0.010)	PC	I^-	11.56	11.36	11.17	24.15	23.15	23.69	23.50
	PC	Br	11.20	10.20	10.19	24.00	23.79	23.71	

dipole interaction and hence displays a similarity to alkaline earth elements. The formation of strong coordinated bonds to sulphur in DT18C6 with the *fd*-configuration of Ln^{2+} in the systems concerned is obviously not realized. Otherwise an abrupt change in the energy parameters in the presence of sulphur-containing ethers would take place, as happens, for instance, in the case of the transition metals (see ref. 66, p. 158).

Figure 23 shows the absorption spectra of the *fd*-transitions in $YbBr_2$ where the effect of the symmetry of the surroundings on the splitting of the Yb^{2+} absorption bands is clearly defined. This effect is mostly defined in the presence of DT18C6, i.e. when the symmetry of the surroundings is low.

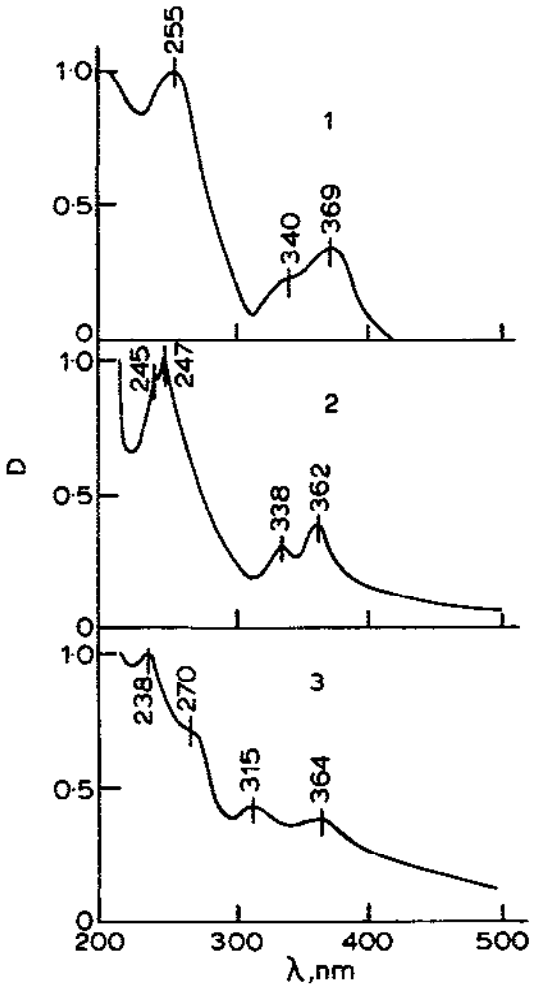

Fig. 23. Influence of crown ethers on the Yb^{2+} absorption spectrum of *fd*-transitions. 1, $YbBr_2$–PC; 2, $YbBr_2$–18C6–PC; 3, $YbBr_2$–DT18C6–PC [47].

Besides the crowns the cryptands are also of interest from the point of view of complex formation. Eu^{2+}, Sm^{2+} and Yb^{2+} are known to form stable complexes with cryptands of various composition [65,76,77]. The most stable are the complexes with 2,2,2-cryptand. The $\log(\beta_{Ln^{2+}}/\beta_{Ln^{3+}})$ ratios range from 2 to 7. The stabilization of Sm^{2+} and Eu^{2+} by cryptands is observed in methanol [78], while in PC the stabilization of Ln^{2+} by cryptands does not take place [78]. This seemed rather surprising because it disagreed with data on complex formation with crown ethers in PC.

Loufouilou and Gisselbrecht [79] carried out a thorough electrochemical study to find reasons for the absence of the stabilization of Sm^{2+} by cryptands in PC. They confirmed the existence of anomalous interaction of Sm^{2+} in PC with these ligands and, using oxidation potentials and values of $\log \beta$ for Sm^{3+} with cryptands, determined $\log \beta$ for Sm^{2+} with cryptands 222,221 and 22 (DA18C6) (Table 15). Comparison of the complex-forming properties of 18C6 and 22 cryptand (DA18C6) having the same dimensions of the ring shows that DA18C6 (22 cryptand) forms stronger complexes than 18C6. However, the authors [79] find no adequate explanation for this fact, though they believe that solvation processes and possible covalent bond formation along with the electrostatic interaction for lanthanide elements may play a role.

(b) Complex formation of uranium(III) with crown ethers

Like Ln^{2+}, trivalent uranium is a strong reducing agent ($E^0_{U^{4+}/U^{3+}} = -0.63$ V). Therefore the question of its stabilization in solution is rather acute. In this respect, the use of crown ethers might be rather efficient because the ionic radius of U(III) (0.1035 nm) correlates well with the size of the cavity of a number of crown ethers. However, as shown in Table 16, 18C6 and its derivatives do not affect the stability of U(III) solutions in water. Slight stabilization is observed in the case of 12C4 and 15C5. Since the absorption spectra of *fd*-transitions of U(III) in the presence and absence of

TABLE 15

Stability constants for samarium complexes with cryptands in PC [79]

Cation	Ligand			
	$\log \beta$			
	222 (1.40 Å)	221 (1.10 Å)	22(DA18C6) (1.40 Å)	18C6 (1.40 Å)
Sm^{3+}	17.3	19.0	16.5	8.1
Sm^{2+}	17.6	15.6	11.2	8.9

TABLE 16

Influence of crown ethers on the oxidation velocity of U^{3+} in water [80] $[U^{3+}] = 0.015$ mol l^{-1}.

	$[U^{3+}]$:[L]	K (s^{-1})	$T_{1/2}$ (h)
UI_3		1.3×10^{-6}	148
UI_3+18C6	1:2	1.5×10^{-6}	128
UI_3+DCH18C6	1:2	1.7×10^{-6}	116
UI_3+DB18C6	1:2	1.9×10^{-6}	101
UI_3+15C5	1:4	9.6×10^{-7}	200
UI_3+12C4	1:4	8.5×10^{-7}	227

crown ethers are identical, one can conclude that the hydrated uranium ion does not form complexes with crown ethers in aqueous solution. The existence in water of weak sandwich complexes is possible in the case of 15C5 and 12C4.

In solutions in organic solvents, characterized by lower dielectric constants and consequently by a lower solvation energy, the molecules of the solvent are replaced by crown ethers, i.e. complex formation processes take place. Complex formation with U(III) was observed in solutions of CH_3CN, PC, THF for all the crown ethers used, confirmed by changes in the absorption spectra of uranium(III) *fd*-transitions in these solvents (Table 17) [80]. Shifts in the absorption bands and their splitting are greater the lower the symmetry of the uranium(III) (Fig. 24). The size of the crown ether ring being the same, the energy parameters of uranium(III) are affected by the solvent and substituents in the crown ether ring and the nature of the donor atoms of the ring. Table 17 shows that the crystal field-splitting parameter for uranium(III), in CH_3CN, changes in the sequence DB18C6 > 18C6 > DCH18C6, i.e. the most stable complexes are formed in DCH18C6, which is accounted for by its most pronounced conformation and steric properties.

The substitution of sulphur atoms for oxygen atoms in the crown ether ring leads to a decrease in the stability of the complexes, while the introduction of =NH groups contributes to the formation of more stable complexes. This is probably related to partial formation of the covalent bond for the divalent lanthanides and uranium(III).

G. SOLID COORDINATION COMPOUNDS OF THE LANTHANIDES AND ACTINIDES IN THEIR LOWER OXIDATION STATES

Solid complexes of the lanthanides and actinides in their lower oxidation states are difficult to obtain due to experimental difficulties related to their

TABLE 17

Energy parameters for U^{3+} in different media (10^3 cm^{-1}) [80] $[U^{3+}] = 0.015$ mol l^{-1}.

Medium	Δ^a	E_{fd}^b
UI_3–PC	13.88	22.85
UI_3–PC–12C6	11.49	22.06
UI_3–PC–15C5	12.01	21.23
UI_3–PC–18C6	12.80	23.00
UI_3–PC–DCH18C6	10.44	21.62
UI_3–PC–DH18C6	13.04	23.24
UI_3–PC–DA18C6	11.56	22.02
UI_3–CH_3CN	12.40	22.73
UI_3–CH_3CN–12C4	12.30	22.31
UI_3–CH_3CN–15C5	11.46	22.13
UI_3–CH_3CN–18C6	10.98	22.32
UI_3–CH_3CN–DB18C6	11.30	21.46
UI_3–CH_3CN–DCH18C6	10.79	22.65
UI_3–CH_3CN–DH18C6	11.94	22.06
UI_3–CH_3CN–DA18C6	10.59	24.11
UI_3–THF	18.03	25.82
UI_3–THF–DCH18C6	14.75	24.87
UI_3–THF–DB18C6	16.32	24.12
UI_3–THF–DT18C6	13.47	23.52

[a] Δ is the crystal field-splitting parameter.

[b] E_{fd} for a free ion of U^{3+} is equal to 27.10×10^3 cm^{-1} [22].

high sensitivity to traces of oxidizing agents and, primarily, atmospheric moisture and oxygen. Therefore, only a limited number of coordination compounds are known in the solid state.

Most numerous are organometallic derivatives. For divalent Sm, Yb and Eu, organic compounds of the type R_2Ln and RLnX were obtained (R = Cp, Cp′, Fc, $C_5H_4M(CO)_3$, CHC=CH, R′C=C, CN, Ar, Alk and others; Cp′ is the substituted cyclopentadienyl ligand). In the case of fully substituted compounds, R_2Ln both σ- and π-bonds are possible between the organic group and the lanthanide atom. In monosubstituted cyclopentadienyl derivatives, the covalency of the Cp–ligand bond is stronger than that in the biscyclopentadienyl compound. Carbonylmetallic derivatives of the lanthanides, where lanthanide–transition metal bonds occur, are also of interest from both theoretical and practical standpoints. Monosubstituted compounds of the type $L(OC)_mMLnX$ and disubstituted compounds $[L(OC)_nM_2]Ln$, where

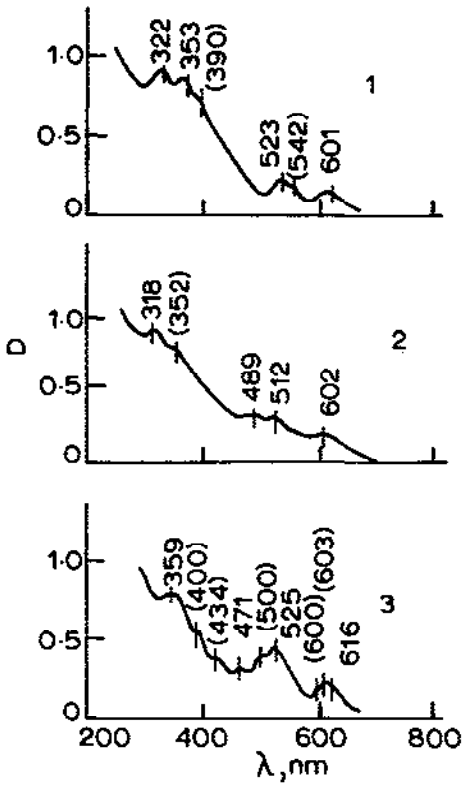

Fig. 24. U^{3+} absorption spectra of *fd*-transitions in PC. 1, $UI_3 \cdot DT18C6$; 2, $UI_3 \cdot 18C6$; 3, $UI_3 \cdot DA18C6$ [80].

Ln = Eu, Sm, Yb, M = Co, Mo, Mn, Re, W, Cr, Fe and others, and X = Cl, Br, I, were obtained.

The formation of organometallic compounds by the actinides in the oxidation state 3+ was reported long ago. The data concerned were reviewed by Mefodieva and Krot [81]. However, there are still no data on organometallic compounds of the divalent actinides.

Since the chemistry of organometallic compounds is very specific, a detailed discussion of this class of coordination compounds of the divalent lanthanides is beyond the scope of this paper. This problem has also been discussed in other exhaustive reviews [82,83].

Since the coordination spheres of the lanthanides are unsaturated, their organometallic compounds are usually in the form of solvates with THF, Et_2O and other organic solvents. However, data on hydrates and solvates of simple lanthanide salts are scarce. We know about $EuBr_2 \cdot H_2O$, which is formed during the hydrolysis of europium dibromide by water vapour present in the air. Moreover, in this case, the hexahydrate is not formed, unlike the

case of strontium dibromide, the hydrolysis of which yields $SrBr_2 \cdot H_2O$, isostructural with $EuBr_2 \cdot H_2O$, and eventually $SrBr_2 \cdot 6H_2O$ [84]. $EuBr_2 \cdot H_2O$ has an orthorhombic symmetry with the lattice parameters $a = 11.46$ Å, $b = 4.291$ Å and $c = 9.20$ Å. The possibility of the existence of the $EuBr_2$ hydrate is explained by a high oxidation potential of the couple Eu^{3+}/Eu^{2+}, which can be realized even in aqueous solutions without oxidation of Eu^{2+}. Unfortunately, already for Yb^{2+} the existence of such a hydrate is problematic. However, $YbCl_2 \cdot THF$ was reported [50] to be formed by the reduction of $YbCl_3$ in THF by metallic lithium in the presence of naphthalene. This compound has a monoclinic symmetry with the lattice parameters $a = 12.59$ Å, $b = 8.519$ Å, $c = 7.290$ Å and $\beta = 102.30^{\circ}$ [85].

(i) Ln^{2+} and U^{3+} compounds with crown ethers

A number of Ln^{2+} and U^{3+} complexes with crown ethers and their derivatives are known [86–90].

The simplest method for obtaining these complexes consists in the interaction of LnI_2 or UI_3 solutions with a solution of the crown ether in THF. The resulting compounds are of different colours; the M:crown ratio is 1:1 or 1:2. Table 18 shows the composition and colour of Ln^{2+} and U^{3+} com-

TABLE 18

Complexes of Ln^{2+} and U^{3+} with crown ethers, and their colours [47,80]

	12C4	15C5		DB15C6	18C6	DB18C6	DCH18C6	DT18C6	DA18C6
	1:2	1:1	1:2	1:1	1:1	1:1	1:1	1:1	1:1
YbI_2	Light yellow	Light yellow	Light yellow		Light green	Greyish-yellow	Light pink	Light pink	Light green
SmI_2	Lilac	Lilac	Lilac		Blue	Blue	Violet	Dark green	Bluish-green
$SmCl_2$					Crimson				
TmI_2					Bluish-green	Bluish-green	Bluish-green	Greyish-brown	Green
$TmCl_2$					Red				
DyI_2					Dark green	Muddy-brown			
NdI_2					Lilac				
UI_3	Greyish-brown	Orange			Red			Brown	Violet
UCl_3		Red [90]		Red [90]	Red [89,90]				
$U(BH_4)_3$					[89]	Orange			

plexes with a number of crown ethers. All these compounds are poorly soluble in THF, but they are soluble in CH_3CN and PC. However, thulium compounds in PC and CH_3CN will be quickly oxidized. The complex with sulphur-containing crown ethers DT18C6 is less stable than that with 18C6. For instance, $TmI_2 \cdot$DT18C6 is oxidized at the drying stage, while $TmI_2 \cdot$18C6 is stable in darkness, but is oxidized in the light, i.e. it is sensitive to light.

Table 19 shows solubility values for some Ln^{2+} and U^{3+} complexes in THF. The introduction of a substituent in 18C6 increases the solubility of the Yb and Sm complexes about 10 times. In Sect. C, data for the solubility products of Ln^{2+} and An^{2+} complexes with 18C6, were determined using the cocrystallization method (Table 2). The SP values for Cf^{2+}, Es^{2+}, Fm^{2+}, and Am^{2+} complexes cannot be determined using the usual method of saturating the solutions due to their high radioactivity and unavailability in weighable quantities. The data obtained using the cocrystallization method showed that the SP values of complexes of these elements were close to those of complexes of the divalent lanthanides and strontium. It is another proof of the fact that Ln^{2+} and An^{2+} are close in terms of their properties to strontium, which is consistent with the size of the ionic radii of these elements.

Table 20 shows decomposition temperatures for some Ln^{2+} and U^{3+} complexes with crown ethers obtained through the thermogravimetric method. Complexes with DB18C6, DCH18C6 and DT18C6 show a decrease in the thermal stability of the compounds compared with 18C6 while for complexes with DB18C6 the thermal stability increases.

Spectroscopic studies with complexes of divalent and trivalent samarium with crown ethers [88] showed that complexes with 18C6 were stronger than those with DT18C6. The appearance in the IR spectra of stretching vibrations of Ln–O points to the coordination of the metal with the ligand by means

TABLE 19

Solubility of Ln^{2+} and U^{3+} complexes with crown ethers in THF at 25 °C (10^{-3} mol l^{-1}) [80]

Crown ether	M:crown	YbI_2	SmI_2	TmI_2	UI_3	$U(BH_4)_3$
12C4	1:2	0.8	0.8		1.1	
15C5	1:1	2.6	2.4		0.6	
15C5	1:2	1.9	1.6			
18C6	1:1	0.2	0.2		0.2	Soluble [89]
DB18C6	1:1	4.5	3.7	4.3		
DCH18C6	1:1	2.8	2.0	2.7		
DT18C6	1:1	3.6	1.5	2.6	2.0	
DA18C6	1:1	1.0	0.9	1.0	0.2	

TABLE 20

Decomposition temperature of the Ln^{2+} and U^{3+} complexes with crown ethers (K) [80]

Crown ether	M:crown	YbI_2	SmI_2	TmI_2	UI_3	UCl_3
12C4	1:2		446		358	
15C5	1:1		433		496	581 [90]
15C5	1:2		450			
18C6	1:1	465	498	451	363	473 [89]
Db18C6	1:1		451			
DCH18C6	1:1		469			
DT18C6	1:1		470			
DA18C6	1:1		518		504	

of the crown ether oxygen atoms. Ln–O stretching vibrations for compounds with 18C6 lie in a region of lower energy compared with sulphur-containing ethers.

Complexes with the composition $LnCl_2 \cdot 18C6$ (Ln–Sm, Tm) are obtained as a result of the exchange of the iodide ion for the chloride during the interaction of $LnI_2 \cdot 18C6$ with LiCl solution in THF, i.e. chloride complexes are more stable than iodide complexes [86].

The reflection spectra of *fd*-transitions of Sm^{2+} with crown ethers are shown in Fig. 25 where the effect of the halide ion and sulphur atoms in the crown ether on the splitting of the absorption bands can clearly be seen.

Crown ether U^{3+} complexes $UCl_3 \cdot 18C6$, $U(BH_4)_3 \cdot 18C6$ [89] as well as $UCl_3 \cdot 15C5$ and DB15C5 [90] were obtained from THF. In addition to thermogravimetric data on these complexes (Table 18) preliminary X-ray crystallographic results of $U(BH_4)_3 \cdot 18C6$ have been reported [89]. They establish that the uranium is actually located inside the crown ether cavity for two of the three different uraniums in the unit cell.

Thus, among the coordination complexes of the lanthanides and uranium in their lower oxidation states, by far the most numerous are halide complexes of these elements with crown ethers. Also of interest are studies of analogous coordination compounds with other anions stable to low oxidation potentials, e.g. with TPB^-, BF_4^-, ClO_4^-. Investigations in this direction are promising.

H. COORDINATION CHEMISTRY OF Ln^{2+} AND An^{2+} WITH AN $f^n d^1$-CONFIGURATION

As mentioned above, all lanthanides and actinides in the oxidation state 2+ may be divided into two groups depending on their electronic configuration. The chemical properties of the first group having an $f^n d^0$-configuration in the divalent state have already been discussed in this paper; these are the most thoroughly studied. As to the second group of divalent lanthanides and

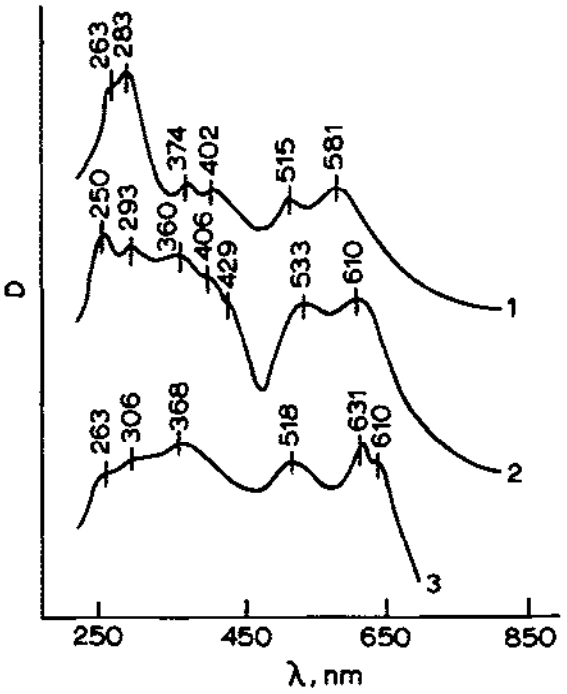

Fig. 25. Reflection spectra of $SmCl_2 \cdot 18C6$ (1), $SmI_2 \cdot 18C6$ (2), and $SmI_2 \cdot DT18C6$ (3) [47].

actinides, which have one unpaired *d*-orbital electron, their properties have rarely been studied. Early work in this direction involved study of oriented cocrystallization of divalent plutonium with $NdBr_2$ [91].

(i) Simple clusters of divalent plutonium and curium

Since the oxidation potentials of the couples Pu^{3+}/Pu^{2+} and Nd^{3+}/Nd^{2+} are almost equal in molten $NdBr_2$, plutonium is qualitatively reduced to its divalent state. The difference in the ionic radii of Nd^{2+} and Pu^{2+} does not exceed 2.7%. This creates favourable conditions for isomorphous cocrystallization of the dibromides of the elements. However, the crystallization process may be hindered by the high complex formation energy of divalent plutonium in melts. This is expected from the fact that divalent plutonium has a different electronic configuration from Am^{2+} and is characterized by an increased hydration energy (by about 2 eV) (see Sect. E.(i)).

The principle of oriented cocrystallization involves the following. A homogeneous mixture of $NdBr_2$ and a microquantity of $PuBr_3$ is placed in a tantalum tube having a diameter of 7 mm and a length of 70 mm, and which has one sealed end. The tube is sealed in argon and placed in a vertical

vacuum furnace equipped with a mechanism for controlled lowering of the tube from the heated zone. After the contents of the tube have melted, it is lowered gradually from the heated zone. As a result, $NdBr_2$ crystallizes in the lower part of the tube. As the tube is lowered, a greater amount of $NdBr_2$ cocrystallizes, the crystallization front always being in equilibrium with the molten portion of the salt. When crystallization is complete, the tube is cut into separate disks which are analyzed for the content of the components.

The distribution of the microelements along the crystallized $NdBr_2$ sample are shown in Fig. 26. Microquantities of Eu and Am, reduced by neodymium to oxidation state 2+, cocrystallize with $NdBr_2$ with a cocrystallization coefficient close to 1.

This is in good agreement with the similarity between the ionic radii of cocrystallizing components and their electronic configurations. The behaviour of Pu^{2+}, is anomalous. As cocrystallization proceeded, its cocrystallization coefficient increased from less than 1 to 4.5 and then started to decrease.

The unusual behaviour of plutonium during cocrystallization with $NdBr_2$ encouraged further study. Towards this end we studied the cocrystallization of $PuBr_3$ with $SmBr_2$, since $NdBr_2$ and $SmBr_2$ are isostructural and the ionic radii of Sm^{2+} and Nd^{2+} differ by no more than 2%. It appeared that Pu^{3+} cocrystallized with $SmBr_2$ with a cocrystallization coefficient below 1, the D

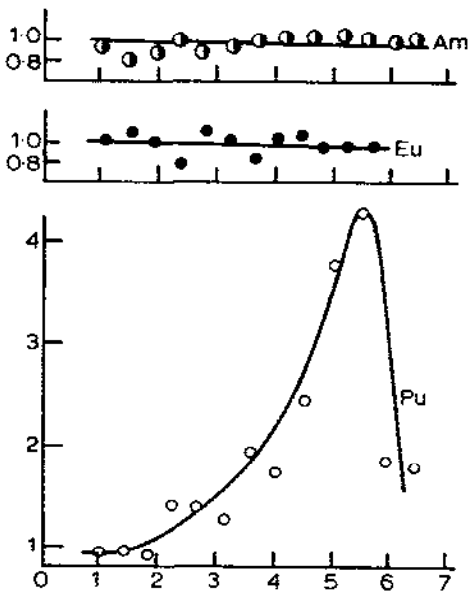

Fig. 26. Distribution of Am^{2+}, Eu^{2+} and Pu^{2+} between the solid phase and the melt under directed crystallization of $NdBr_2$ [92].

value remaining constant along the crystallization zone and the maximum of the cocrystallization coefficient being absent.

So the anomalous behaviour of Pu^{2+} requires explanation. Mikheev et al. [91] believe that the cocrystallization of Pu^{2+} occurs in the form of dimers. Initially the amount of dimers formed is small and the cocrystallization coefficient of Pu^{2+}, due to its high complex formation energy, is below 1. However, with time the dimerization process occurs but at a slow rate due to the low concentration (10^{-4} mol.%) and low diffusion coefficient of Pu in molten salts. Ultimately, as the crystallization proceeds, a greater amount of Pu is dimerized. At the same time, the cocrystallization coefficient increases. Simultaneously, the plutonium concentration in the melt declines, thereby hindering dimerization. This mechanism explains the existence of a maximum during oriented cocrystallization.

On the other hand, dimerization shouled obviously result in an increase in the oxidation potential of the Pu^{3+}/Pu^{2+} couple. Mikheev et al. [92] determined the oxidation potential of Pu^{3+}/Pu^{2+} using ^{238}Pu, whose half life is 278 times lower than that of ^{239}Pu. This gave an opportunity to decrease the Pu concentration by about 100 times.

Experiments showed that the oxidation potential of the Pu^{3+}/Pu^{2+} couple (using ^{238}Pu) was 0.16 V lower than that in experiments with ^{239}Pu. Hence the dimerization energy of Pu^{2+} is 0.3–0.4 eV at a temperature of 1173 K. Moreover, Mikheev et al. [93] showed that, in the presence of weighable quantities of ^{239}Pu (10^{-4} mol.%), the oxidation potential of the Cm^{3+}/Cm^{2+} couple increased by the value by which the oxidation potential of the Pu^{3+}/Pu^{2+} had decreased when ^{238}Pu was used instead of ^{239}Pu. The authors believe that this result may be explained by the formation of the mixed dimers $(CmPu)^{4+}$.

However, the oxidation potential of the pair Pm^{3+}/Pm^{2+} does not change in the presence of divalent ^{239}Pu. This is because Pm^{2+} has an $f^n d^0$ electronic configuration and is unable to form mixed dimers.

Thus, the presence of an electron in the *d*-orbital of the lanthanides and actinides brings their properties closer to the properties of *d*-elements, which are known to form clusters. Dimers also belong to clusters.

(*ii*) *Condensed lanthanide and actinide clusters*

Much attention has been paid to the study of lanthanide clusters by Simon [94–96]. He obtained a number of compounds in which the degree of oxidation of the lanthanides varies from 1.0 to 2.0. Most clusters synthesized by these authors, were obtained by the solid synthesis technique. However, of special interest are compounds of the type MX and M_2X_3 obtained through interaction of metal with the melt of the respective trihalide. Thorough

investigations showed that these compounds represent so-called condensed clusters whose structure and properties are considered in greater detail in reviews by Simon [95,96]. Analogous compounds with the actinide elements are unknown.

In contrast to isolated clusters, containing a backbone in the form of chains formed by M–M bonds, an additional M–M bond appears between the chains in condensed clusters. The bond distance between the metal atoms in the chain and between chains is different.

Clusters of this type were obtained for Gd, Lu, Tb, Y and other elements.

The possibility of substitution of separate metal atoms by atoms of another metal to form a condensed mixed cluster is very promising. this problem first arose [97,98] during a study of the cocrystallization of various elements with Gd_2Cl_3.

(a) Mixed condensed lanthanide and actinide clusters of the M_2Cl_3 type

Following from the work of Simon and coworkers, some lanthanides are not able to form condensed clusters by interaction of their melts with a molten trihalide. Eu, Sm, Yb and other elements belong to this group. This may imply that synthesis provides no conditions for the solid phase of the cluster to be formed. However, this does not imply that the formation of this cluster by the above elements is impossible in principle. If it is so, the lanthanide in question must take part in cocrystallization during the formation of a matrix, e.g. Gd_2Cl_3.

As mentioned above, the formation of Gd_2Cl_3 occurs through interaction of metallic gadolinium with $GdCl_3$ at a temperature close to the melting point of $GdCl_3$. Corbett showed that, under these conditions, Gd^0 partially dissolves in $GdCl_3$, its solubility being ≈ 2 mol.% at a temperature of 883 K. It was established [99] that dissolution of Gd^0 is accompanied by the formation of Gd^{2+} ions. Thus, a redox system is formed where, in the presence of $GdCl_3$ in the melt, the lanthanides and actinides will be reduced to the oxidation state 2+ with their degree of reduction depending on their standard oxidation potentials (Table 21). Table 21 shows that some lanthanides and actinides are reduced almost completely to their divalent states, some are reduced partially, and some remain in the oxidation state 3+.

Three problems were to be solved during the study of cocrystallization of these elements with Gd_2Cl_3:

(1) whether the lanthanides and actinides can cocrystallize with Gd_2Cl_3 if they have an $f^n d^0$-configuration in the divalent state;

(2) whether Ln^{2+} and Ac^{2+} can cocrystallize with Gd_2Cl_3 if they have an $f^{n-1}d^1$-configuration;

(3) in which oxidation state *f*-elements cocrystallize with the Gd_2Cl_3 matrix.

TABLE 21
The M^{3+}/M^{2+} ratio in the system Gd^0–$GdCl_3$ at 833 K [100]

Ln	An	*d*-element	$E^0_{M^{3+}/M^{2+}}$ (V) (NHE)	$[M^{3+}]/[M^{2+}]$
La			−2.94	51
Ce			−2.92	39
Pr			−2.84	14
Nd			−2.62	0.76
Pm			−2.44	7.2×10^{-2}
Sm			−1.5	3.1×10^{-5}
Eu			−0.34	6.2×10^{-14}
Gd			−2.85	16
Tb			−2.83	12
Dy			−2.56	0.35
Ho			−2.79	7.1
Er			−2.87	20
Tm			−2.22	4.0×10^{-3}
Yb			−1.18	4.6×10^{-9}
Lu			−2.72	2.8
	U		−2.54	0.27
	Np		−2.91	34
	Pu		−2.59	0.51
	Am		−2.28	8.7×10^{-3}
	Cm		−2.78	6.2
	Cf		−1.63	3.5×10^{-5}
		Y	−2.92	39

The answer to the first question was reported [98,100,101] and it was shown that Eu, Yb, Nd, Dy, Tm, Am and Cf did not cocrystallize with Gd_2Cl_3. All these elements in the divalent state had an $f^n d^0$ electronic configuration. Following from Table 21, they are reduced, with a different degree of reduction from the oxidation state 2+, according to the conditions of the experiment. Thus, cocrystallization of these elements occurs neither in the di- nor the trivalent state.

Further studies [100] showed that Np, Pu, Cm, Tb and Y, i.e. elements which in the $GdCl_3$ melt in the form of M^{2+} have an $f^{n-1}d^1$-configuration, cocrystallized with Gd_2Cl_3. Since the degree of reduction of these elements under the conditions of the experiment is different (Table 21), the question of the valency of Ln and An in cocrystallization remains open. The maximum transition to the Gd_2Cl_3 phase was observed in the case of Np, Y and Tb (Table 22), i.e. for the elements with the lowest degree of reduction, and vice

TABLE 22

Distribution of Ln and An during cocrystallization with Gd_2Cl_3 in the system Gd^0–$GdCl_3$ [101]

M	Electronic configuration M^{2+} in melt	% in Gd_2Cl_3	M	Electronic configuration M^{2+} in melt	% in Gd_2Cl_3
Eu	f^7d^0	2	Ce	f^1d^1	6
Yb	$f^{14}d^0$	2	Tb	f^8d^1	68
Nd	f^4d^0	2	Lu	$f^{14}d^1$	50
Am	f^7d^0	2	Np	f^4d^1	76
Cf	$f^{10}d^0$	2	Pu	f^5d^1	38
			Cm	f^7d^1	38

versa, Pu, having the highest degree of reduction, is least of all trapped by the Gd_2Cl_3 phase.

For a better understanding of the formation of the Gd_2Cl_3 cluster, Mikheev et al. [101] considered two mechanisms:

$$\begin{array}{l} Gd^0 + 2\,GdCl_3 \rightarrow 3\,GdCl_2 \\ \underline{3\,GdCl_2 \rightarrow Gd_2Cl_3 + GdCl_3} \\ Gd^0 + GdCl_3 \rightarrow Gd_2Cl_3 \end{array} \qquad (21)$$

$$\begin{array}{l} Gd^0 \rightarrow Gd^{3+} + 3e^- \\ 2\,GdCl_3 + 3\,e^- \rightarrow Gd_2Cl_3 + 3\,Cl^- \\ \underline{Gd^{3+} + 3\,Cl^- \rightarrow GdCl_3} \\ Gd^0 + GdCl_3 \rightarrow Gd_2Cl_3 \end{array} \qquad (22)$$

Using these two mechanisms, cocrystallization equations were obtained taking into account the solubility of metallic Gd^0 in $GdCl_3$ (K), the ratio between di- and trivalent forms of macro- and microcomponents, determined by the $\Delta E^0_{M-\mu}$ value, i.e. by the difference in standard oxidation potentials of the pairs M^{3+}/M^{2+} for Gd(M) and microcomponent (μ), and the distribution of the microcomponent between molten $GdCl_3$ and the solid phase Gd_2Cl_3 (λ).

For the first mechanism

$$\ln\left(\frac{a}{a-x}\right) = \frac{2(1+k)}{1+k\exp[\Delta E^0_{M-\mu}/(RT/F)]}\lambda_1 \ln\left(\frac{2b}{2b-y}\right) \qquad (23)$$

and for the second mechanism

$$\ln\left(\frac{a}{a-x}\right) = \frac{2(1+k)\exp[\Delta E^0_{M-\mu}/(RT/F)]}{1+k\exp[\Delta E^0_{M-\mu}/(RT/F)]}\lambda_2 \ln\left(\frac{2b}{2b-y}\right) \qquad (24)$$

where a and b are the contents of the macro- and microcomponents in the system, and x and y are their contents in the cluster phase. If $\Delta E^{0}_{M-\mu}=0$, the two equations coincide:

$$\ln\left(\frac{a}{a-x}\right)=2\lambda\ln\left(\frac{2b}{2b-y}\right) \tag{25}$$

In this case it is impossible to choose between the first or the second mechanism of cluster formation. At the same time, one should note that the first mechanism implies the existence of divalent gadolinium. In this case, if the microcomponent, which also reduces to the oxidation state 2+ and has an $f^{n-1}d^1$ electron configuration, is introduced into the system, its cocrystallization ability will be determined by the share of this element in the divalent state. The second mechanism implies the participation in cocrystallization of the trivalent form of the element, therefore in this case the opposite tendency should be observed, i.e. cocrystallization worsens by increasing the share of the reduced form of the element.

Since we speak about the elements with similar ionic radii, their cocrystallization coefficients are close. Table 23 shows the λ_1 and λ_2 values for the elements in question calculated according to eqns. (23) and (24), respectively. From these data it follows that only λ_2 coefficients are in agreement with each other. Therefore, the authors conclude that the formation process of Gd_2Cl_3 occurs according to the second mechanism, i.e. with the trivalent form of the element participating in cocrystallization.

Moreover, as shown above, the $f^{n-1}d^1$ electronic configuration of the divalent form of the element plays a crucial role in cluster formation.

These conclusions are in agreement with the data on the magnetic properties of Gd_2Cl_3, Mössbauer and photoelectron spectroscopy of Gd_2Cl_3 [94], and with the $(sp)d$-character of the additional 1.5 electrons for each gadolinium atom [96]. The presence of the $(sp)d$-character of the additional electrons in the metal atoms of the cluster implies a specific role for d-electrons and the possibility of the splitting of the d-level in the ligand field. In this respect, the behaviour of Pr, Ho and Er in the formation of mixed cluster with

TABLE 23

Cocrystallization coefficients (dimensionless) of elements with Gd_2Cl_3 [101]

Element	λ_1	λ_2
Np	1.16	2.21
Pu	0.07	2.03
Cm	0.70	1.73

Gd_2Cl_3 is very interesting. These elements in a free state and also in the melt [20] have an $f^n d^0$ M^{2+} configuration. However, following from Figs. 1 and 2, they are close to Gd^{2+} and Tb^{2+} in terms of their energy parameters having an $f^{n-1}d^1$-configuration. If the ligand field splitting in the solid matrix is assumed to be higher than that in the melt, one may expect the stabilization of Pr, Ho and Er in an $f^{n-1}d^1$-configuration, and, consequently, the formation of them of mixed clusters with Gd_2Cl_3. Actually, it appeared that Pr, Ho and Er transfer to the Gd_2Cl_3 phase with λ_2 coefficients (eqn. (24)) being 0.50, 1.01 and 1.32, respectively. Thus, all these elements cocrystallize due to their $f^{n-1}d^1$-configurations, stabilizing in the ligand field of the Gd_2Cl_3 matrix.

At the same time, the cocrystallization coefficients of Ho and Er differ from the cocrystallization coefficient of Pr by more than a factor of 2. The cocrystallization of La, Ce, Pr, Y and Lu was studied to determine the effect of the ionic radius on the formation of a mixed cluster. All these elements in their divalent states have an $f^{n-1}d^1$ electronic configuration with the exception of Y^{2+}, which has a $[Kr]d^1$ configuration. As shown in Table 24, in this group of elements the ionic radii decrease from La to Lu. Moreover, for elements with ionic radii smaller than that of Gd^{2+}, the λ_2 value is close to or higher than 1. An increase in the ionic radius of Pr^{3+} by 5.5% as compared with Gd^{3+} decreases λ_2 twofold.

Further increase in the radii of Ce and La results in an abrupt decrease in the cocrystallization of these elements with the Gd_2Cl_3 cluster. Thus, in the system $Gd_2(Ln)Cl_3$, there is an upper mixability limit depending on the radii of the lanthanide elements.

Finally, studies of the chemistry of the actinides and lanthanides with $f^{n-1}d^1$-configurations show that there is a specific relation and similarity

TABLE 24

Dependence of the cocrystallization coefficient (λ_2) on the ionic radius of M^{3+} [100]

Element	$R_{M^{3+}}$ (nm)	λ_2
La	0.1061	0.04
Ce	0.1034	0.1
Pr	0.1013	0.5
Gd	0.0938	
Tb	0.0923	1.6
Ho	0.0894	1.0
Er	0.0881	1.3
Lu	0.0848	2.5
Y	0.0900	1.9

between these elements and trivalent Y and, obviously, Sc, which is manifested in their ability to form dimers and condensed clusters.

I. CONCLUSION

Following from the above data, Ln and An exhibit properties of the elements of the *s*-series in their lower oxidation states. Thus, monovalent mendelevium is the closest analogue of K^+, and Ln^{2+} and An^{2+} are analogues of strontium. However, the presence of *f*-electrons in Ln and An makes their properties rather characteristic. This is shown in the ability of Eu^{2+}, Yb^{2+} and Es^{2+} to form outer-sphere coordination compounds with the TPB ion, an observation probably, related to partial delocalization of the *f*-electron.

The extreme case of electron delocalization consists in its transition into the *d*-orbital and formation of an $f^{n-1}d^1$ electronic configuration. In this electronic configuration, Ln and An become analogues of Y and Sc and exhibit a tendency for the formation of dimers and condensed clusters.

Studies of the coordination chemistry of Ln and An in their lower oxidation states started recently, and we can express our hope for unexpected discoveries in this field.

REFERENCES

1 V.I. Spitsyn and L.I. Martynenko, Coordination Chemistry of Rare Earth Elements, Izd. MGU, Moscow, 1973, p. 13.
2 W.T. Carnall, in K.A. Gschneidner, Jr. and Le Roy Eyring (Eds.), Handbook on the Physics and Chemistry of Rare Earths, Vol. 3, North-Holland, New York, 1979, p. 171.
3 W.T. Carnall, Actinides-85, Vol. 2, Elsevier Sequoia, Lausanne, 1986, p. 1.
4 K.E. Johnson and J.K. Sandoe, J. Chem. Soc. A, (1960) 1694.
5 A.N. Kamenskaya, K. Buketinska and N.B. Mikheev, Zh. Neorg. Khim., 24 (1979) 1139.
6 A.N. Kamenskaya, Zh. Neorg. Khim., 29 (1984) 439.
7 R.J. Silva, W.J. McDowell and O.L. Keller, Inorg. Chem., 13 (1974) 2233.
8 W.J. McDowell, O.L. Keller and P.E. Dittner, J. Inorg. Nucl. Chem., 38 (1976) 1207.
9 M.N. Litvina, Ph.D. Thesis, MGU, Moscow, 1970.
10 T.V. Bettger, Ph.D. Thesis, MGU, Moscow, 1976.
11 N.A. Kostromina, Complexonates of Rare Earth Elements, Izd. Nauka, Moscow, 1980, p. 187.
12 D. Braun, Halogenides of Lanthanides and Actinides, Atomizdat, Moscow, 1972, p. 161.
13 G. Meyer, Chem. Rev., 88 (1988) 93.
14 K. Kramer, T. Schleid, M. Schulze, W. Urland and G. Meyer, Z. Anorg. Allg. Chem., 575 (1989) 67.
15 Y.P. Souchez, M. Malki, H. Bärninghausen, K. Federkeil and W. Stüber, J. Less Common Met., 127 (1987) 61.
16 T. Schleid and G. Meyer, J. Less Common Met., 127 (1987) 161.
17 R.D. Baybarz, L.B. Asprey and C.E. Strause, J. Inorg. Nucl. Chem., 34 (1972) 3427.
18 R.D. Baybarz, J. Inorg. Nucl. Chem., 35 (1979) 483.
19 C. Keller, GIT Fachz. Lab., 31 (1987) 1149.

20 N.B. Mikheev, Naturwissenschaften, 76 (1989) 107.
21 N.B. Mikheev, Radiokhimiya, 30 (1988) 297.
22 K.L. Vander Sluis and L.J. Nugent, J. Opt. Soc. Am., 64 (1974) 687.
23 L.R. Morss, in A.J. Bard, R. Parsons and J. Jordan (Eds.), Standard Potentials in Aqueous Solution, Marcel Dekker, New York, 1985, p. 587.
24 G.T. Seaborg, Science, 103 (1946) 649.
25 G.T. Seaborg, Nucleonics, 5 (1949) 16.
26 N.B. Mikheev, V.I. Spitsyn and G.V. Ionova, Radiokhimiya, 28 (1986) 82.
27 L. Henderson and F. Kraček, J. Am. Chem. Soc., 47 (1927) 738.
28 A. Ratner, J. Chem. Phys., 1 (1933) 789.
29 N.B. Mikheev, I.A. Rumer and O.N. Ilyushenko, Radiokhimiya, 13 (1971) 745.
30 N.B. Mikheev and I.A. Rumer, Radiokhimiya, 13 (1971) 746.
31 N.B. Mikheev, R.A. Dyachkova and I.A. Rumer, J. Radioanal. Chem., 30 (1976) 527.
32 N.B. Mikheev, A.N. Kamenskaya and S.A. Kulyukhin, Radiokhimiya, 30 (1988) 56.
33 V.I. Spitsyn, N.B. Mikheev and A.N. Kamenskaya, Radiokhimiya, 24 (1982) 615.
34 V.S. Urusov, Theory of Isomorphous Mixability, Izd. Nauka, Moscow, 1977.
35 N.B. Mikheev and L.M. Mikheeva, Zh. Neorg. Khim., 7 (1962) 671.
36 N.B. Mikheev, A.N. Kamenskaya and S.A. Kulyukhin, Radiokhimiya, 28 (1986) 204.
37 N.B. Mikheev, A.N. Kamenskaya and S.A. Kulyukhin, Radiokhimiya, 28 (1986) 588.
38 N.B. Mikheev, A.N. Kamenskaya and S.A. Kulyukhin, Radiokhimiya, 27 (1985) 839.
39 N.B. Mikheev, I.A. Rumer and L.N. Auerman, Radiochem. Radioanal. Lett., (1983) 317.
40 W.C. Martin, R. Zalubas and L. Hagan, Natl. Stand. Ref. Data Ser. Natl. Bur. Stand., 60 (1978).
41 V.I. Minkin (Ed.), Lanthanides, Izd. Rostov.GU, Rostov-na-Donu, 1980, p. 28.
42 N.B. Mikheev and I.A. Rumer, Radiokhimiya, 29 (1987) 112.
43 F. David, J. Less Common Met., 121 (1986) 27.
44 N.B. Mikheev, A.N. Kamenskaya and S.A. Kulyukhin, Radiokhimiya, 30 (1988) 213.
45 A.N. Kamenskaya, J. Drozhdzhinsky and N.B. Mikheev, Radiokhimiya, 22 (1980) 247.
46 A.N. Kamenskaya, J. Drozhdzhinsky and N.B. Mikheev, Radiokhimiya, 23 (1981) 264.
47 N.B. Mikheev and A.N. Kamenskaya, Radiokhimiya, 31 (1989) 95.
48 A.N. Kamenskaya, S.A. Kulyukhin and N.B. Mikheev, Radiokhimiya, 28 (1986) 701.
49 A.N. Kamenskaya, N.B. Mikheev and A.N. Strekalov, Zh. Neorg. Khim., 28 (1983) 1711.
50 K. Rossmanitch, Monatsh. Chem., 110 (1979) 109.
51 A.N. Kamenskaya, N.B. Mikheev and N.P. Kholmogorova, Dokl. Akad. Nauk SSSR, 266 (1982) 393.
52 A.N. Kamenskaya, N.B. Mikheev and N.A. Konovalova, Zh. Neorg. Khim., 22 (1977) 2130.
53 A.N. Kamenskaya, N.B. Mikheev and N.A. Konovalova, Zh. Neorg. Khim., 22 (1977) 3243.
54 N.B. Mikheev, A.N. Kamenskaya and I.A. Rumer, Radiokhimiya, 25 (1983) 153.
55 A.N. Kamenskaya, N.B. Mikheev and N.P. Kholmogorova, Zh. Neorg. Khim., 28 (1983) 2499.
56 A.N. Kamenskaya, N.B. Mikheev, S.A. Kulyukhin, Zh. Neorg. Khim., 30 (1985) 615.
57 S.A. Kulyukhin, N.B. Mikheev, A.N. Kamenskaya, Radiokhimiya, 30 (1988) 416.
58 V.V. Kuznetsov, Usp. Khim., 55 (1986) 1409.
59 N.B. Mikheev, S.A. Kulyukhin, I.A. Rumer and A.N. Kamenskaya, Radiokhimiya, 30 (1988) 218.
60 N.B. Mikheev, A.N. Kamenskaya and S.A. Kulyukhin, Radiokhimiya, 27 (1985) 837.
61 N.B. Mikheev, A.N. Kamenskaya and S.A. Kulyukhin, Radiokhimiya, 27 (1987) 341.
62 M. Bonnin, C. Musikas and P. Vitorge, 12 Journees des Actinides, May 1982, Orsay, France, 1982, p. 68.
63 J.L. Dye, in J. Jortner and N.R. Kestner (Eds.), Electrons in Fluids, Springer-Verlag, Berlin, Heidelberg, 1973, p. 77.
64 J.-C.G. Bunzli and D. Wessner, Coord. Chem. Rev., 60 (1984) 191.

65 J.-C.G. Bunzli, in K.A. Gschneidner, Jr. and Le Roy Eyring (Eds.), Handbook on the Physics and Chemistry of Rare Earths, Vol. 9, Elsevier, New York, 1987, p. 321.
66 M. Khiraoka, Crown Compounds. Properties and Application, Izd. Mir, Moscow, 1986.
67 Y. Shiokawa and Sh. Suzuki, Bull. Chem. Soc. Jpn., 57 (1984) 2910.
68 H. Yamana, Bull. Chem. Soc. Jpn., 55 (1982) 2615.
69 Y. Shiokawa, T. Kido and Sh. Suzuki, J. Radioanal. Nucl. Chem. Lett., 96 (1985) 249.
70 H. Yamana, T. Mitsugashira, Y. Shiokawa, A. Sato and S. Suzaki, J. Radioanal. Chem., 76 (1983) 1.
71 S.A. Kulyukhin, A.V. Mayorov, A.N. Kamenskaya and N.B. Mihkeev, Radiokhimiya, 31 (1989) 48.
72 N.B. Mikheev and B.F. Myasoedov, in A.J. Freeman and C. Keller (Eds.), Handbook on the Physics and Chemistry of the Actinides, Vol. 3, Elsevier, New York, 1985, p. 347.
73 J. Massaux and J.R. Desreux, J. Am. Chem. Soc., 104 (1982) 2697.
74 J. Massaux, J.R. Desreux, C. Delchambre and G. Duyckaerts, Inorg. Chem., 19 (1980) 1893.
75 A.N. Kamenskaya, S.A. Kulyukhin, E.S. Levchenko and V.N. Kalinin, Koord. Khim., 16 (1990) 868.
76 O.A. Gansow, A.R. Kauser, K.M. Triplett, M.J. Weaver and E.L. Yee, J. Am. Chem. Soc., 99 (1977) 7087.
77 E.L. Yee, O.A. Gansow and M.J. Weaver, J. Am. Chem. Soc., 102 (1980) 2278.
78 M.C. Almasio, F. Arnaud-Neu and M.J. Schwing-Weill, Helv. Chim. Acta, 66 (1983) 1296.
79 E.L. Loufouilou and J.P. Gisselbrecht, Can. J. Chem., 66 (1988) 2172.
80 S.A. Kulyukhin, A.N. Kamenskaya, N.B. Mikheev and L.N. Auerman, Radiokhimiya, 33 (1991) 10.
81 M.P. Mefodieva and N.N. Krot, Compounds of Transuranium Elements, Izd. Nauka, Moscow, 1987.
82 I.P. Beletskaya and G.Z. Suleimanov, Metalloorg. Khim., 1 (1988) 10.
83 W.J. Evans, Adv. Organomet. Chem., 24 (1985) 131.
84 J.M. Naschke and H.A. Eick, J. Inorg. Nucl. Chem., 32 (1970) 2153.
85 G. Liu and H.A. Eick, Inorg. Chem., 27 (1988) 2161.
86 A.N. Kamenskaya and N.B. Mikheev, Inorg. Chim. Acta, 110 (1985) 27.
87 S.A. Kulyukhin, N.B. Mikheev and A.N. Kamenskaya, Radiokhimiya, 32 (1990) 26.
88 A.N. Kamenskaya, N.B. Mikheev and S.A. Kulyukhin, The 3rd Conference on the Chemistry of Macrocyclic Compounds, Ivanovo, 1988, p. 254.
89 D.C. Moody, R.A. Penneman and K.V. Salazar, Inorg. Chem., 18 (1979) 208.
90 D.C. Moody, A.J. Zozulin and K.V. Salazar, Inorg. Chem., 21 (1982) 3857.
91 N.B. Mikheev, I.A. Rumer and M.Z. Kazakevich, Radiokhimiya, 28 (1986) 773.
92 N.B. Mikheev, M.Z. Kazakevich and I.A. Rumer, Radiokhimiya, 30 (1988) 268.
93 N.B. Mikheev, I.A. Rumer and M.Z. Kazakevich, Radiokhimiya, 30 (1988) 270.
94 A. Simon, Ann. Chim. Fr., 7 (1982) 539.
95 A. Simon, Naturwissenschaften, 71 (1984) 171.
96 A. Simon, Angew. Chem., 20 (1981) 1.
97 N.B. Mikheev, A. Simon, H. Mattausch and C. Keller, Z. Naturforsch., 42 (1987) 666.
98 N.B. Mikheev, A. Simon and G. Mattausch, Radiokhimiya, 30 (1988) 314.
99 N.B. Mikheev, L.N. Auerman and I.A. Rumer, Zh. Neorg. Khim., 28 (1983) 1329.
100 N.B. Mikheev, A.N. Kamenskaya and I.A. Rumer, Int. Conf. Actinides-89, Sept. 1989, Tashkent, USSR, 1989, p. 135.
101 N.B. Mikheev, A.N. Kamenskaya and I.A. Rumer, Radiochim. Acta, 48 (1989) 219.